UNIVERSITÀ DEGLI STUDI DI PADOVA
DIPARTIMENTO DIA INGEGNERIA INDUSTRIALE
CORSO DI LAUREA MAGISTRALE IN INGEGNERIA DEI MATERIALI

Tesi di Laurea Magistrale in
Ingegneria dei Materiali

High Precision Fast Scanning Calorimetry on the FlashDSC 2+ Device

Relatore: ***Prof. Irene Calliari***
Correlatore: ***Prof. Stephan Pogatscher***

Laurendo: ALESSANDRO MINOTTO
n° 1157249

ANNO ACCADEMICO 2019 - 2020

Omnia tempus habent.

Abstract

In this work a MEMS-based fast scanning calorimeter is used to measure the specific heat of pure metals. The instrument in question is the Flash DSC 2+, the latest model of fast scanning calorimeter, from Mettler Toledo (Switzerland). It can support two different sensors: the MultiSTAR UFS 1 and the recently introduced MultiSTAR UFH 1. Both sensors will be employed in the evaluation of pure lead's specific heat: the choice of the same metal makes it possible a comparison between the two, while the purity allows a reliable comparison with the literature's values. Furthermore, pure aluminium's specific heat is measured on the MultiSTAR UFH 1 sensor to exploit its full potential. MultiSTAR UFH 1 sensor differs from the MultiSTAR UFS 1 since the former enables to reach higher temperatures compared to the latter.

With both metals, several samples with different masses (ranging from 10 ng to 5 µg) have been analysed at different heating rates (100, 1000, 2000 K/s). Two different corrective methods are tested with the purpose of obtaining a better specific heat evaluation. A quantitative comparison will be performed, enabling to formulate hypotheses on how the precision of the measurement is affected by the different parameters.

The first and the second chapters will be devoted to the description of the technology behind fast scanning calorimetry, before going into the description of the equipment and materials used for the trials. The third and the fourth chapters will deal with the experimental set-up, the collection, and the processing of the data generated by the measurements.

This experimental work was carried out at the Lehrsthul für Nichteisenmetallurgie, the Chair of Nonferrous Metallurgy of Montanuniversität Leoben, Austria, under the supervision of Prof. Stefan Pogatscher.

Riassunto

In questo lavoro un calorimetro a scansione differenziale ultrarapida, che utilizza la tecnologia MEMS, è stato usato per misurare il calore specifico di metalli puri. Lo strumento in questione è il Flash DSC 2+, il più recente modello di calorimetro a scansione ultrarapida della Mettler-Toledo (Svizzera). Esso può operare con due diversi sensori: il MultiSTAR UFS 1 ed il MultiSTAR UFH 1, recentemente introdotto. Entrambi i sensori sono stati impiegati per la misurazione del calore specifico del piombo puro: la scelta di utilizzare un unico metallo consente di effettuare un paragone tra i due, mentre la purezza garantisce una comparazione affidabile con i valori presenti in letteratura. In aggiunta, il calore specifico dell'alluminio puro è stato misurato su sensori MultiSTAR UFH 1, per sfruttare a pieno il loro potenziale. Il sensore MultiSTAR UFH 1 differisce dal sensore UFS 1 per la possibilità di raggiungere temperature più elevate rispetto a quest'ultimo.

Con entrambi i metalli, più campioni con pesi diversi (che variano fra i 10 ng ed i 5 μg) sono stati analizzati a varie velocità di riscaldamento (100, 1000, 2000 K/s). Due metodi correttivi differenti sono testati allo scopo di ottenere una migliore stima del calore specifico. È stata inoltre realizzata un'analisi quantitativa dei risultati, che permette di formulare ipotesi su come i vari parametri influiscano sul grado di precisione della misurazione.

Il primo ed il secondo capitolo sono dedicati alla descrizione tecnologia che sta alla base della tecnica della calorimetria a scansione ultrarapida, per poi entrare nel dettaglio della strumentazione e dei materiali utilizzati nelle prove. Il terzo ed il quarto capitolo trattano invece la preparazione sperimentale, la raccolta e l'elaborazione dei dati originati dalle misurazioni.

Questo lavoro sperimentale è stato svolto preso il Lehrsthul für Nichteisenmetallurgie, il Dipartimento di Metallurgia dei Metalli non Ferrosi della Montanuniversität di Leoben, Austria, sotto la supervisione del Prof. Stefan Pogatscher.

Contents

Chapter 1

Introduction to the Fast DSC principles

This chapter will introduce the technology and the theoretical principles typical of the Fast DSC techniques. A comparison with the regular DSC will contextualize its capabilities, discussing both the pros and cons of both techniques. A brief historical excursus will open the chapter, presenting the continuous development that lead to development of Differential Scanning Calorimetry.

1.1 History

In 2006, the ICTAC (International Confederation for Thermal Analysis and Calorimetry) put forward the following definition of Thermal Analysis:

"A group of techniques that study the relationship between a sample property and its temperature".

In these terms, the first time a heat quantity was measured as a function of temperature is traced back to 1887, when the French chemist Henry Louis Le Chatelier (1850-1936) attempted to discriminate between various minerals in clay using heating-rate curves [1][2]. He placed a Pt:Pt-10%Rh thermocouple in a sample of clay, which was then constantly heated up to 1000°C in a furnace [3]. The thermocouple output was recorded on a photographic plate every two seconds thanks to a mirror galvanometer: the distance between the images offered an indication of the heating rate. Ten minutes were necessary for the temperature to reach 1000°C, giving an average heating rate of 4°C every two seconds. To graduate the thermocouple, the fusion and boiling temperatures of water (100°C), sulphur (448°C), selenium (665°C) and gold (1045°C) were used as fixed points. The results of this experiment showed that during the heating phase, decelerations corresponding to dehydration alternated to sudden accelerations which were due to the production of exothermic phenomena. The numerous samples used by Le Chatelier could be summed up in five types, whose behaviour is shown in the figure at the top of the next page (Fig. 1.1 –.

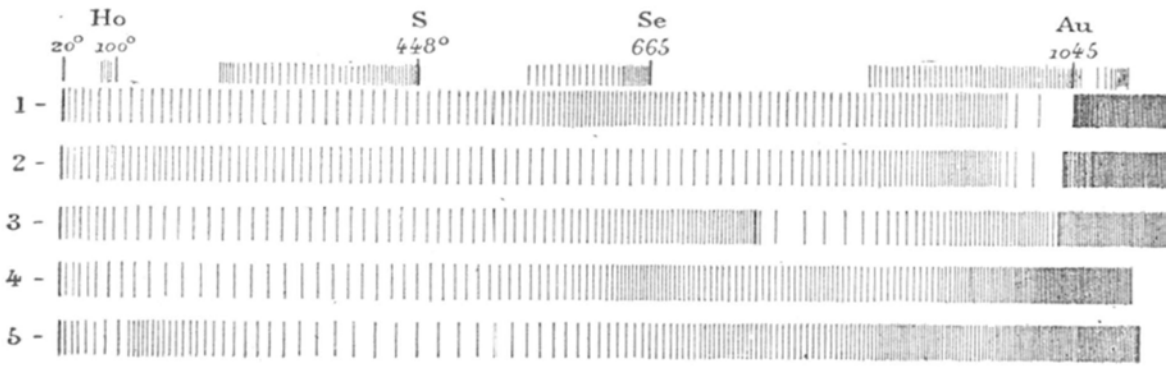

Fig. 1.1 – Graphical representation obtained as a result during the measurements performed by Le Chatelier on clay samples, with graduating elements above [3].

Despite the rudimentary technique, thermal analysis had begun. In 1899, another milestone in the improvement of thermal analysis techniques was set. The British scientist William C. Roberts-Austen devised the first classical differential thermal analysis (DTA) arrangement [4], thus generating the first DTA curve: a sample and a reference crucible of the same type were arranged in a single heat source and subjected to a common temperature program; two thermocouples respectively inserted in the sample and in the inert reference material would then measure the temperature difference between them. Even if this design allowed the thermal effect to be detected, the measure of the enthalpy could only be of qualitative nature, and not quantitatively determined.

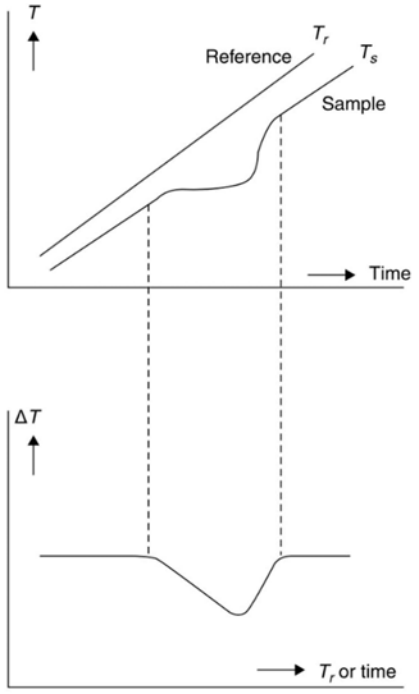

Fig. 1.2 – DTA curve, obtained by the subtraction of the Reference Temperatures from the Sample Temperature.

A quantitative analysis was made possible by E. S. Watson et al., who in 1964 proposed the first Differential Scanning Calorimeter (DSC) for Differential Thermal Analysis [5]. The innovation of this measuring instrument lay in the possibility to quantitatively measure the transition energy of the sample analysed in a direct and precise way.

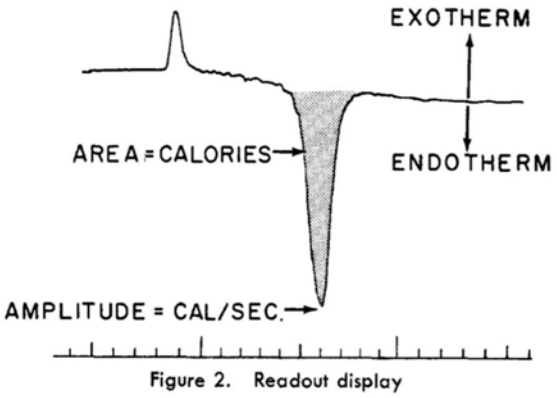

Fig. 1.3 - Graphical description of the DSC output [5].

The DSC technique can detect endothermic and exothermic effects, determine peak areas (transition and reaction enthalpies), determine temperatures that characterize a peak or other effects, and measure specific heat capacity. The notation presented above (Fig. 1.3) is still actual, and it is taken from the original publication dated 1964. What changed in DSC techniques from them on are the performance of the instruments, that are strongly related to the technology behind the instrument, as it will be explained in the next section.

1.2 Technology and Theoretical Principles

At the base of the Differential Scanning Calorimetry functioning there is the reference/sample relation. Both the elements undergo to the same time-temperature program: the sample is placed in a crucible, meanwhile the reference usually consists in an empty crucible. The crucibles have to embodies the following characteristics:

- They should be inert, to avoid any reaction with the sample;
- They should not manifest any physical transition in the temperature interval of interest;
- They must prevent the contamination of the sensor by the sample;
- Their heat capacity should be as little as possible, to ensure a small signal time constant;
- They have to guarantee an optimum thermal conductivity to minimize temperature gradients in the sample.

The temperatures of the reference and the sample are continuously monitored, so every temperature difference that occurs between them is the manifestation of a thermal effect occurring on the sample. Two resistors, one per element, compensate and measure the amount of heat needed to balance the thermal effect occurring on the sample (Fig. 1.4 –.

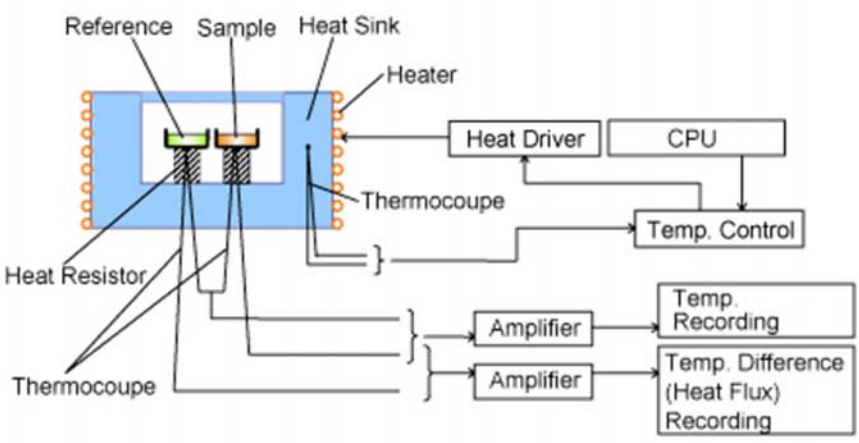

Fig. 1.4 – Working scheme of a power compensated DSC.

Many efforts have been made in the last 20 years in the improvement of the Differential Scanning Calorimeters, most of them addressed to the extension of the scanning rates, set at 10°C/min for the regular DSC techniques.

Among the benefits that can be achieved by reducing the time scale, there is the possibility to study reorganization mechanism that occurs only at certain speeds of heating or cooling. Many manufacturing processes includes high cooling rates, on the order of 100-10.000 °C/s, like blow molding and injection molding for polymers, and welding or quenching for metal, to give some examples. With the current DSC techniques those rates cannot be achieved.

The factor that limits the scanning rates is represented by the thermal lag that occurs between the temperature measured by the thermocouple and the actual temperature of the sample/crucible system, and it is due to the thermal inertia of the latter. Theoretically, a reduction in the size of the pan and in the sample mass allows an increase of the scanning rate. In fact, rates between 200°C/min and 750°C/min can be achieved by analysing samples with a mass that ranges from milligrams to micrograms. It is a common practice to refer to these techniques as “High Performance DSC”, or HPer DSC.

A great leap forward has been made with the adoption of Micro-Electro-Mechanical Systems (MEMS)-based sensors. Such technology allows to get rid of the pan, by placing the sample straight on a membrane. The opposite side of the membrane holds all the necessary electronics components, such the resistor and the thermopile. All the techniques based on this technology fall into the definition of *Fast Scanning Calorimetry* [6].

A schematic representation of a calorimeter can be provided by the figure below (Fig. 1.5 -.

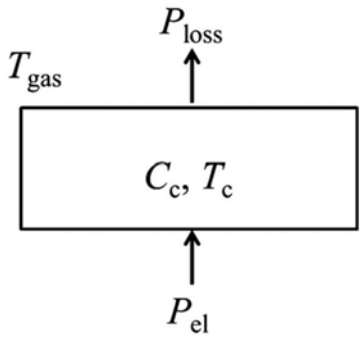

Fig. 1.5 - Schematic representation of a non-adiabatic calorimeter.

Where P_{el} is the electric power provided as source of heat, and P_{loss} sums up the thermal losses. P_{loss} is a function of the temperature difference (ΔT) that exists between the gas (T_{gas}) and the calorimeter (T_c), and the thermal resistance that there is between the two media R_{CG}:

$$P_{loss} = -\frac{\Delta T}{R_{CG}}$$

At equilibrium the energy balance is:

$$P_{el} = P_{loss}$$

But in a non-stationary state, also the heat capacity of the calorimeter C_c comes into play together with β, that represents scanning rate dT_c/dt, according to:

$$P_{el} = P_{loss} + C_c\beta$$

- In the heating phase the heat capacity of the calorimeter should be as little as possible, since for a given P_{el} and P_{loss}, high heating rates can be obtained by minimizing C_c,
- When it comes to cooling, high cooling rates can be obtained only if high P_{loss} affects the system, since P_{el} can be null at most. P_{loss} can be increased by decreasing the gas temperature (greater ΔT) and decreasing the resistivity R_{CG}.

To achieve the two points, a cold gas is used as cooling medium and a thin membrane is employed to ensure a small heat capacity. The same membrane that holds the sample, it holds also the electronic components needed for the performance of the measurement. The heating is provided by a resistor, while temperature is detected by the use of thermopiles. Thermopiles are preferred instead of resistive thermometers because they do not need any current, which would inevitably generate a discrete amount of heat [7].

Chapter 2

Instrumentation & Materials

After having introduced in the first chapter the principles of the Fast DSC technique, this second chapter will discuss in detail the capabilities of the instrument that has been used for the data collection. Two different type sensors will be presented, together with the nature of the samples which have been analysed.

2.1 The Flash DSC 2+

The Flash DSC 2+ is the latest instrument of Mettler Toledo for the *fast differential scanning calorimetry*. It can support both MultiSTAR UFS 1 sensor and MultiSTAR UFH 1 sensor, and it can achieve cooling rates [8] that range from:

- 0,1 to 4.000 K/s (6 to 240.000 K/min) with the MultiSTAR UFS 1;
- 0,1 to 40.000 K/s (6 to 2.400.000 K/min) with the MultiSTAR UFH 1;

and as regards the heating rates:

- 0,1 to 40.000 K/s (6 to 2.400.000 K/min) with the MultiSTAR UFS 1;
- 0,1 to 50.000 K/s (6 to 3.000.000 K/min) with the MultiSTAR UFH 1.

These rates make the Flash DSC 2+ able to deal with non-equilibrium phenomena, in contrast with the regular DSC techniques. The ultra-high heating rates can suppress the reorganization processes, while the ultra-high cooling rates can allow the formation of materials with defined structural properties.

To run the Flash DSC 2+ (Fig.2.1) it is required the aid of the following instruments:

- an *optical microscope*,

  that comes together with the calorimeter and it's placed just above the sensor chip housing. It is used both for the sample preparation and both for the placing the sample on the sensor;

- an *Huber two-step intracooler TC100*,

  that is connected to the Flasch DSC 2+ with the purpose to cool down up to -100°C the gas flowing in the measuring chamber;

- a source of *dry-gas*,

  needed to purge the measuring chamber. Argon with 5 N purity has been used for all the experiments;

- a *flow-meter*,

  that regulates the incoming flow of dry-gas: it has been set at 60 ml min^{-1}.

Fig. 2.1 - The Flash DSC 2+, front view.

Moreover, the instrument works in synergy with S**TA**R^{e}, a dedicated software for calorimetry provided by Mettler Toledo. With it, it is possible to:

- set the operative temperatures of the Flash DSC 2+;
- create the thermal methods;
- launch the experiments and monitor their trend in real time
- collect the data and evaluate the different curves collected;
- store in its database both the row data and the evaluations performed.

From now on, the terminology *method* will indicate a sequence of heating, cooling, or isothermal segments that, when performed on the sensor, constitute the experiment itself. The maximum number of segments per each method is 200, and each segment can have its own heating rate and sampling frequency. The minimum duration of a single segment is 1 ms, while the overall duration of the experiment cannot exceed 50 hours. As a trade-off between data resolution and size, the following rule has been applied for all the experiments (Tab. 2.1).

Tab. 2.1 - Sampling frequency and heating/cooling rate correlation.

Heating/Cooling Rate β [K s^{-1}]	**Sampling Frequency [Hz]**
1	10
$1 < \beta \leq 10$	100
$10 < \beta \leq 100$	1.000
$100 < \beta \leq 10.000$	10.000

At high sampling frequencies, data transfer from the Flash DSC module to the STAR^{e} software becomes slower due to amount of data generated in short period of time. A sequence of multiple segments with a frequency of 10.000 Hz can exceed the limitation due to data transfer: for this reason, the methods composed by multiple segments at 10.000 Hz have been limited to 10 heating and cooling cycles. In case more than 10 cycles of measurement are needed, the method is launched as many times consecutively until the desired number of heating cycles is reached. The method under consideration is automatically performed as soon as the data transfer of the previous one is ended. Tab. 2.1 shows the sampling frequency adopted for every heating rate.

2.2 UFS & UFH sensors

Both the UFS-1 and the UFH-1 chips are made up by a 5,0 mm × 3,3 mm × 0,3 mm ceramic plate, with an opening that host two identical membranes. The membranes consist of silicon-nitride (Si_3N_x) and silicon oxide, and its purpose is to hold the sample on one side while incorporating the resistor and the thermocouples on the other (Fig. 2.2).

In addition to these elements, a thin aluminum coating is deposited beneath the sample area in order to homogenize the temperature profile by enhancing thermal conductivity.

A 300 µm thick silicon frame is interposed between each membrane and the ceramic frame, and its serves as heat sink providing thermal inertia to the cold junction of the thermopile.

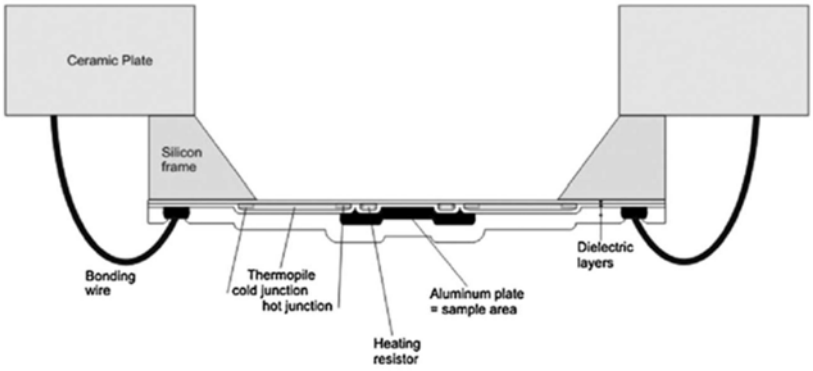

Fig. 2.2 - Schematic representation of sensors UFS-1 and UFH-1.

The sensor communicates with the instrument through a series of gold-plated pins (Fig. 2.3). A clamping ring mechanism with a fixed rotation angle allows to always apply the same tightening torque.

Since the sensor support is exposed to air during the removal and placement procedures, it is recommended to wait until its temperature reach 15 °C.

Ice formation on the pins must be avoided, otherwise the signal could be disturbed or absent at all and consequent water derived from the melting could harm the instrument itself.

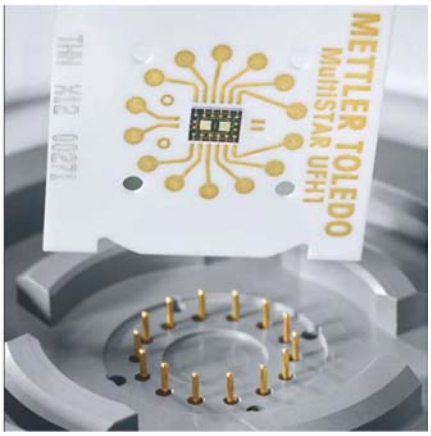

Fig. 2.3 - Sensor-Instrument coupling.

2.2.1 MultiSTAR UFS-1

The MultiSTAR UFS-1 sensor is characterized by a membrane that measures about 1,6 mm × 1,6 mm in width and about 2 μm in thickness.

The aluminum coating has with of 0.5 mm diameter (Fig. 2.4) and 0.5 μm thickness [9].

- T_{max} = 500 °C
- Heating rate range: 0,1 to 40.000 K/s
- Cooling rate range: 0,1 to 4.000 K/s
- Applied sample mass range: 0,1 to 10 μg
- Time costant: 1 ms

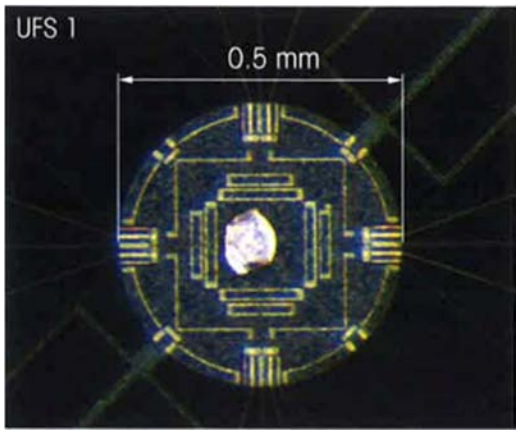

Fig. 2.4 - MultiSTAR UFS 1 sensor, the scale bar indicates the active area.

2.2.2 MultiSTAR UFH-1

The MultiSTAR UFH-1 sensor, where H stands for High temperature, is characterized by a membrane that measures about 1,6 mm × 1,6 mm in width.

The aluminum coating has with of 0.1 mm diameter (Fig. 2.5.)

- T_{max} = 1000 °C
- Heating rate range: 0,1 to 50.000 K/s
- Cooling rate range: 0,1 to 40.000 K/s
- Applied sample mass range: 0,05 to 5 μg
- Time costant: 0,2 ms

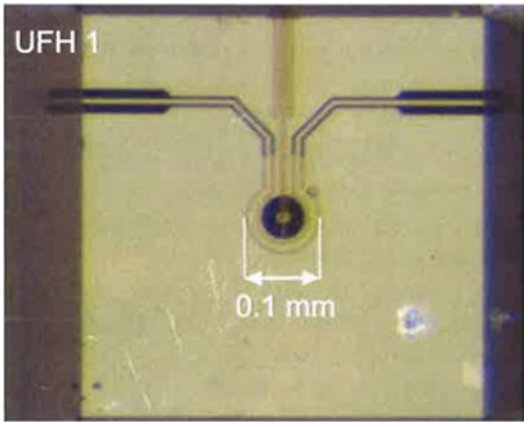

Fig. 2.5 - MultiSTAR UFH 1 sensor, the scale bar indicates the active area.

2.3 Samples

Since the Flash DSC 2+ is part of broader project focused on metallurgic characterization, the choice of the reference substances falls on metals. UFS and UFH sensors are able to track the thermal behavior of a sample among a fixed range of temperatures that spreads from -100°C to 450°C for the UFS and from 100°C to 900°C for the UFH: this constraint narrows the availability of elements to the following list (Tab. 2.2).

Tab. 2.2 - List of the pure metals with melting temperature below 1000°C.

Metal	T_m (°C)
Hg	-38,87
Ga	29,76
In	156,4
Sn	231,9
Pb	327,4
Zn	419,5
Al	660,1
Ag	961,8

2.3.1 Selection of the Metals

The temperature of melting has been chosen as a selection criterion: the metals with the melting point more close to the maximum operative temperature of the sensor are preferred. This is needed in order to have the broader temperature interval on which evaluate the metal at the solid state.
(Fig. 2.6]. shows at which temperature the fixed scanning rates are achieved, that is recognizable by the plateau. The curves in the picture are obtained with N_2 gas, that has a lower cooling power compared to Ar, and empty sensor: compared to the set-up that will be used in this work, the cooling rates are misleading, and the heating rates are not affected by the thermal inertia of the sample. What remains remarkable is that, at scanning rates proper to the instrument, heating and cooling rates stabilization always occur and interest a defined (although limited) interval of temperatures.

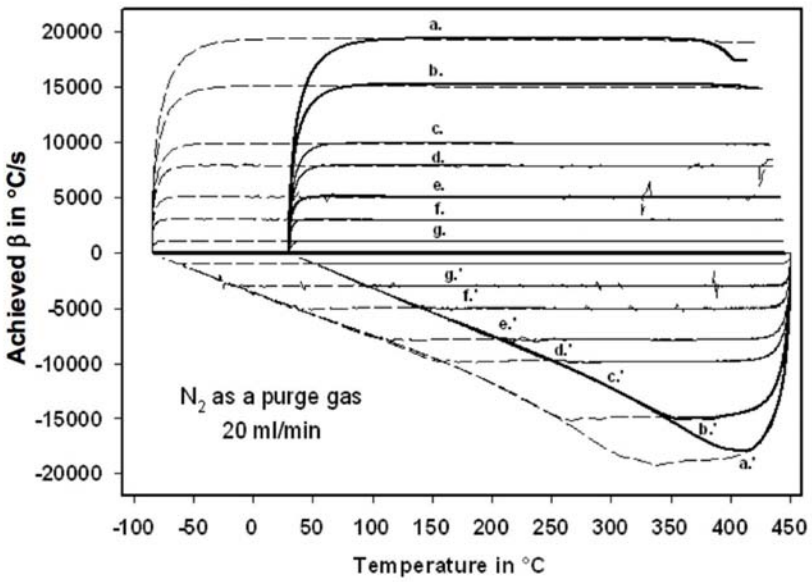

Fig. 2.6 - Achieved scan rates from 20 000 to 10 °C/s versus achieved empty sample side temperature [10].

In the case of the UFS sensor, Zinc has a melting temperature that almost matches the maximum operative temperature of the sensor. On the other hand, it is also characterized by a high vapour pressure, that in the light of the high surface/volume ration and the permanence at high temperature could offset the sample's mass. Lead, even if its melting temperature is 90 °C lower than Zinc, it is supposed not to be affected by weight loss over long time at high temperature, and for this reason it is chosen for the comparison between the two sensors.

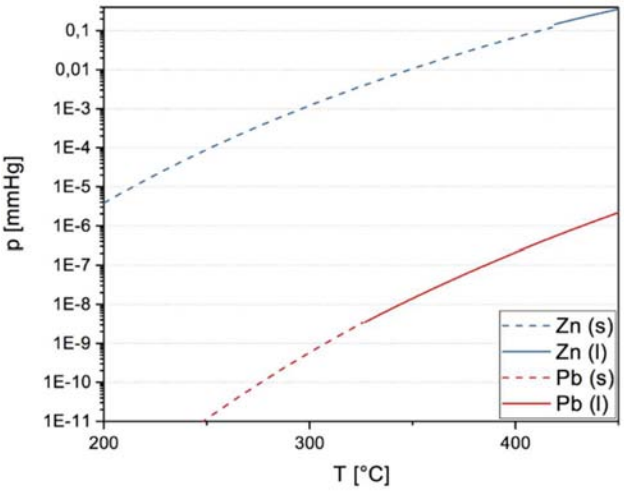

Fig. 2.7 – Vapour pressure of pure Zinc and pure Tin, as a function of temperature. The values related to solid state are represented by the dotted line, while the values of the liquid state are represented by the solid line.

Moreover, pure Al has been used to test the UFH sensor at its full capabilities. In this work the Ag option has been arbitrary rejected, even if its melting could be theoretically feasible.

The choice of pure metals as object of study is dictated by the certainty of their composition, in this regard all the metals used have a 4N degree of purity or more: in this way the comparison with the abundant literature values is extremely reliable (Tab. 2.3).

Tab. 2.3 - List of the metal used, with purity and thickness of the foil of origin.

Metal	Purity [%]	Thickness [µm]
Pb	99,998	100
Al	99,999	38

2.3.2 Properties of the Metals

Mass determination occurs via the melting peak evaluation. The enthalpy of fusion (H_f), together with the measure of the heat provided to the melting peak, is needed for the computation of the sample mass (Tab. 2.4*[11]*.)

Tab. 2.4 – Thermal properties related to the melting peak evaluation [11].

Metal	T_m [°C]	L_m [kJ/mol]	M [g/mol]	H_f [J/g]	ρ [g/cm^3]	h_f [J/cm^3]
Pb	327,4	4,81	207,20	23,21	11,3	262
Al	660,1	10,47	26,98	388,1	2,70	1048

For information and further discussion, in Tab. 2.5 are reported other thermal properties of the two metals.

Tab. 2.5 - Other thermal properties.

Metal	C_p [mJ/g K]	ρ [g/cm^3]	c_p [mJ/cm^3 K]	λ [W/m K]	α [mm^2/s]	CTE [µε/K]
Pb	129	11,3	1457	33,6	23,0	28,9
Al	897	2,70	2421	247	102	23.1

Chapter 3

Thermal Analysis Methods

This chapter deals with both the experimental set-up, and the subsequent data collection and manipulation. The procedures of sensor calibration and sample preparation will be described in the experimental part, meanwhile all the consequent handling of the data collected will be presented in the second part. Furthermore, two different models of heat loss estimation will be described and implemented.

3.1 Experimental

The experimental set-up is intended as a list of actions that precede and lead to the measurement itself. Some of them are mandatory, such as the sensor conditioning and calibration, some other are arbitrary, like the sample preparation that varies with the type of material under investigation. Lastly, the coupling between the sample and sensor give space to execution of recommended practices, that are meant to achieve the optimal thermal contact.

3.1.1 Sensor Conditioning

In chronological order, the conditioning procedure comes first. It requires the sensor support to be in thermal equilibrium, so it is recommended to have the intracooler switched off for at least the previous 5 hours. During the conditioning, Argon gas flows and the sensor is heated up to its maximum operating temperature, for three main reasons:

- its functionality is checked;
- at the maximum operating temperature, possible errors due to memory effects are eliminated;
- the electrical resistance of the heater is determined.

3.1.2 Sensor Correction

During the sensor correction, or more precisely the thermocouple correction procedure, the thermocouple signal is corrected against the current cold junction temperature. To do this, the sensor support temperature must be stabilized at the ready temperature.

3.1.3 Sample Preparation

The pure metal in the form of a thin foil is placed on a microscope slide. Particular care is given to the cleanliness of every surface that comes in contact with the sample, since small traces of organic compounds can alter its handling (e.g. fingerprint residuals). Once under the microscope, the metal is hand-cut with a sharp blade to the desired volume and picked up with a thin bristle. The microscope slide is removed, giving access to the sensor, and the focus is adjusted.

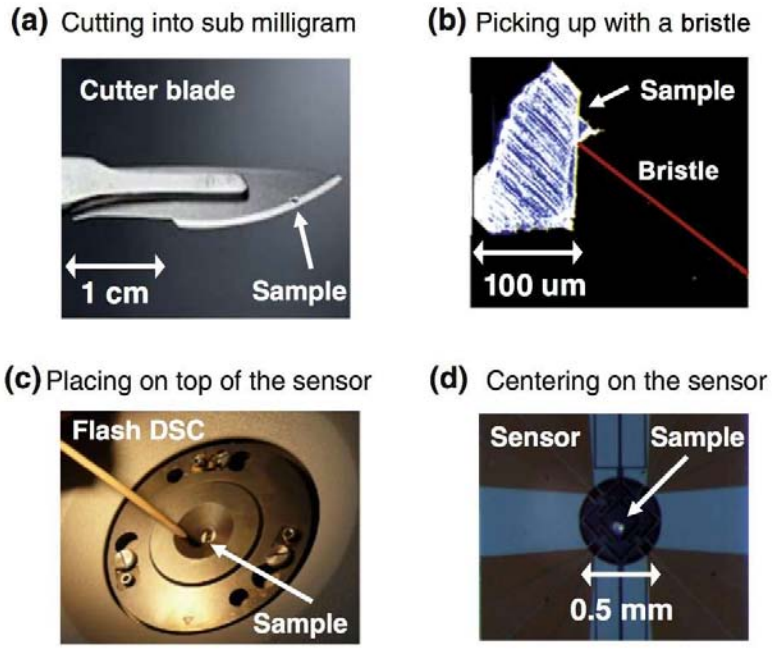

Fig. 3.1 - From "a" to "d" is shown the procedure of obtainment and placement of the sample.

The reason of the bristle is found in its flexibility, that allows to get in contact with the membrane without damaging it. Contact with the membrane occurs during the centering of the sample on the sensor, because it must be placed on the active area.

3.1.4 Sample Stabilization

Once placed on the active area of the sensor, the sensor housing is covered with a lid and the chamber is purged with Argon gas. Aim of the first experiment is to melt the metal in order to establish the optimum thermal contact. The method consists in a first slow heating, to avoid sudden evaporation phenomena that could move the sample away from the center. After the first heating segment, a temperature above the one of melting is kept by an isothermal segment for the duration of about one minute, and then a sequence of heating and cooling segments performs multiple melts and solidifications (Fig. 3.2).

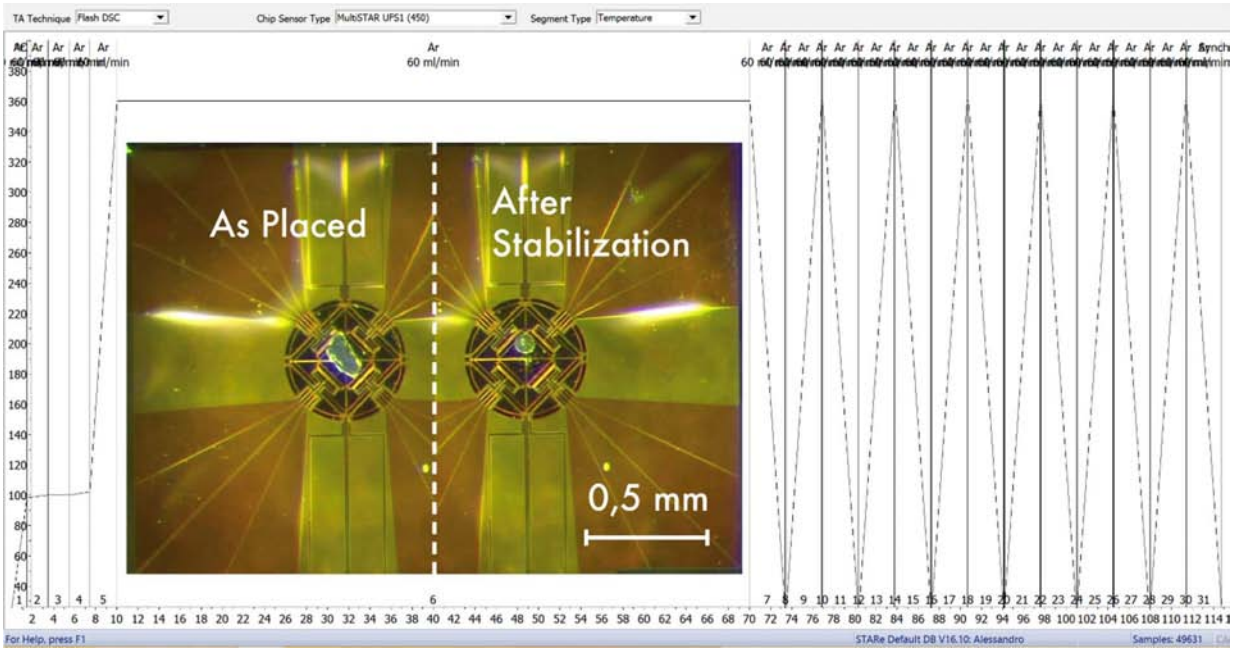

Fig. 3.2 - Sample L, as cut and after stabilization. The segments are the thermal method employed.

The role of the isothermal segment is to allow the liquid sample to reach a stable shape, in line with its tendency of minimization of its surface / volume ratio [12].

Lastly, a sequence of melts offers the possibility to check the nature of the melting. If the peak seems not to be uniform between the various iterations, a subsequent sequence of melts and solidification is performed until a certain degree of repeatability is observed.

The following figures shows how the stabilization is manifested, both in a qualitative way (Fig. 3.3) and in a quantitative way (Fig. 3.4).

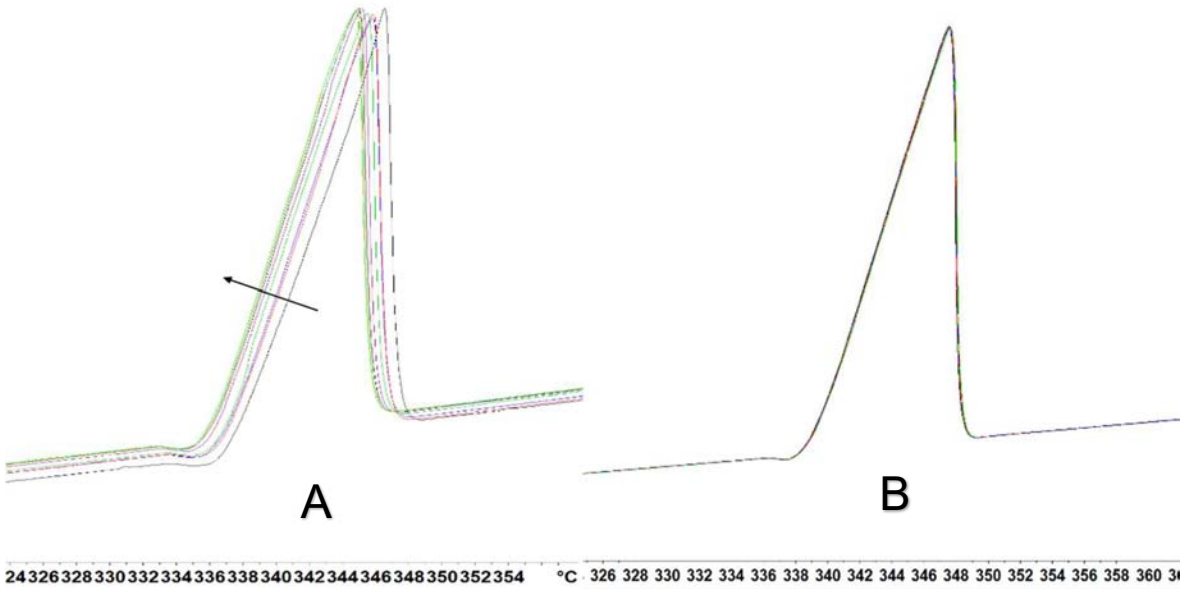

Fig. 3.3 - Sample S, melting peak evolution (A) and stabilization (B).

It is noteworthy how the heat of fusion stabilizes around a fixed value after the spherical shape is reached. Generally, the isothermal segment is sufficient for the sample to stabilize. Fig x represent an exception that occurred because of the large mass the sample (S). Specifically, the lengthening of time helps in the graphical description of the phenomenon.

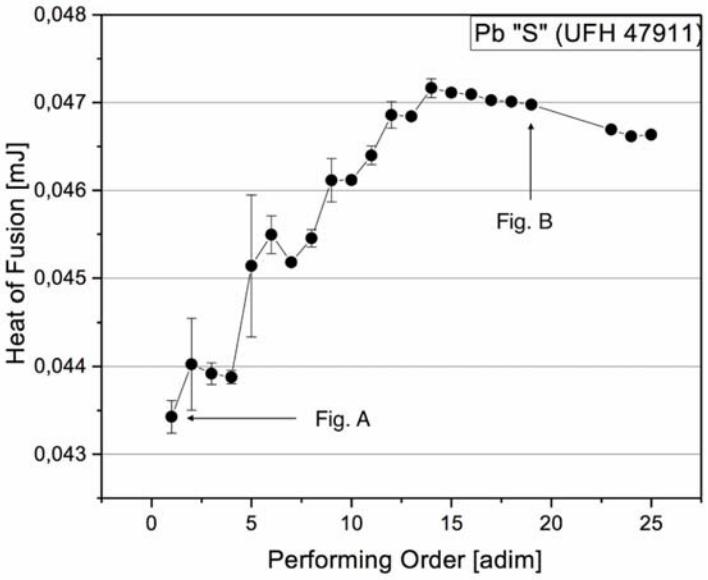

Fig. 3.4 - Sample S, evolution of the measured heat of fusion over time.

3.1.5 Data Collection

Aim of the data collection is the evaluation of the *specific heat*, that can be defined as "*the amount of heat per unit mass required to raise the temperature of a body"*. Its dimensional description is the following:

$$\boldsymbol{Cp} = \frac{[J]}{[K][g]}$$

In a single step manipulation, by multiplying and dividing for the time, it is possible to follow back the definition of specific heat C_p up to the calorimetric parameters ϕ, β and m:

$$\boldsymbol{Cp} = \frac{[J]}{[K][g]} = \frac{[J]}{[s]}\frac{[s]}{[K]}\frac{1}{[g]} = \frac{\boldsymbol{\phi}}{\boldsymbol{\beta}\,\boldsymbol{m}}$$

Where:

$$\boldsymbol{\phi} = heat\ flux\ \left[\frac{J}{s}\right]$$

$$\boldsymbol{\beta} = heating\ rate\ \left[\frac{K}{s}\right]$$

$$\boldsymbol{m} = mass\ [g]$$

In the following subchapters, each component of the specific heat equation will be discussed in detail. The magnitude of the variables involved is hereby listed:

- the heat flux ϕ, always expressed in mJ, will vary between some millijoules and their fractions;
- the heating rate β , expressed in K/s, will vary from 1 to 10.000 K/s;
- the mass m, expressed in µg, will vary between some micrograms and some nanograms.

Each experiment is based on heating and cooling the sample at given rates. Put together, one stage of heating and one stage of cooling form a cycle: a single experiment is made up by a multiple repetition of the particular heating and cooling cycle. To check the repeatability of the measurement, it has been chosen to perform 10 to 30 cycles per experiment. As introduced in

chapter 2.1, some experiments have been split in many different sub experiments (generally 3) for data transfer reasons: the data coming from the different sub experiments have treated as a unique experiment.

All the experiments are performed by the same operator, and every series of experiments executed on a sample has been done in a single day. In case the same sample has been analysed in a second occasion, it will be properly notified in its description.

3.2 Data Curation

During the acquisition, the sampling frequency is constant, making the data-point equidistant in terms of time. The heating rate is kept, on average, constant by the heat-compensation mechanism, but locally it is subject to minimal perturbations. These perturbations make the data-point not equidistant in terms of sample's temperature: to better handle the successive arithmetic operations, the temperature values are truncated to zero decimal digits and all the values related to the same temperature (heating & cooling rates and heat flux) are averaged into a single data point.

For each experiment an averaged heating curve is obtained by averaging all ith heating curves, together with its one-sigma standard deviation. The same process is done with the cooling curves.

3.2.1 The Mass

Due to the small size of the samples, mass estimation has to be done via measurement of thermal effects: in this case, the enthalpy of fusion is exploited. Multiple meltings (10 or more) are performed, and the averaged value is taken. The advantage of averaging the curves is the possibility of obtaining a smoother curve, with consequent better-defined beginning and end of the melting peak. In Fig. 3.5 is shown the worst case scenario, when a small mass sample of Pd is measured on a MultiSTAR UFS 1 sensor, and noise affects the measurement of the peak. The red line is the result of the averaging of all the measured curves, and the beginning and the end of the melting peak are clearly defined.

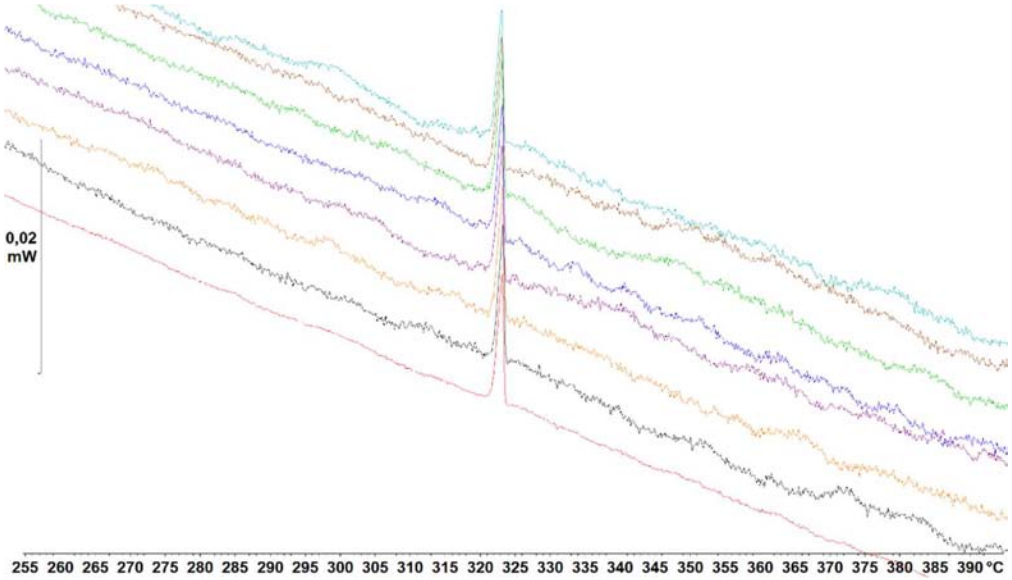

Fig. 3.5 - Melting peak evaluation: from top (light blue) going down (black), the curves collected during the measurements. Bottom (in red), the curve resulting from the averaging of the collected ones.

3.2.2 The Speed Rate

The speed rate β is defined by difference in temperature over a fixed amount of time:

$$\beta = \frac{dT}{dt}$$

In this work it is evaluated point by point with the following formula:

$$\beta_i = \frac{(T_i - T_{i-1})}{(t_i - t_{i-1})}$$

Where T_i is the sample temperature at the t_i time. This has been done to get a better estimation of the term during the stabilization process that occur at the begging of any temperature segment, see Fig. 2.6.

3.2.3 The Heat Flow

Until now the relation between the heat flow and the specific heat has been treated as an ideal model, but this is not the more precise way to deal with it. Even if the sample and the reference are placed in the same chamber and therefore in the same conditions, some differences in the P_{loss} term do always occur. In this situation, the measured heat flow can be described as the sum of two contributes: one is the specific heat of the sample, and the other is a term which gives an account for the discrepancy in the thermal losses.

$$\phi = m * C_p * \beta + \phi_1$$

Where m is the sample mass, C_p is the specific heat capacity of the sample, β is the heating rate and ϕ_1 is the term that stands for the heat losses. Since ϕ_1 is not negligible, it needs to be estimated and subtracted from the measured heat flow as below:

$$C_p = \frac{\phi - \phi_1}{m\,\beta}$$

Thermal losses' estimation is performed using two different approaches, termed *slow correction* and *symmetry correction* for ease of reference [13].

Slow Correction

The first to be described is the *slow correction*: in a stationary state, when the heating rate β is equal to zero, the heat flow is made up just by thermal losses and there is no contribution to the specific heat capacity of the sample.

$$\lim_{\beta \to 0}(m * C_p * \beta + \phi_1) = \phi_1$$

In other terms: the heat flux due to the thermal losses is independent from β, and it is just function of the temperature since the weight and the size of the different dissipation mechanism change.

For this reason, a slow measurement (with scan rate of 1 K/s) has been performed for each experiment.

Symmetry Correction

The second approach is represented by the *symmetry correction*: in a conservative system, the heat provided during the heating should equal the heat released during the cooling phase:

$$m * C_p * \beta + m * C_p * (-\beta) = 0$$

Making the average heat flux, ϕ_{avg}, null:

$$\phi_{avg} = \frac{\left(m * C_p * \beta \right) + (m * C_p * (-\beta))}{2} = 0$$

But in a non-conservative system, where thermal losses occur, the average heat flux ϕ_{avg} takes the form:

$$\phi_{avg} = \frac{\left(m * C_p * \beta + \phi_1 \right) + (m * C_p * (-\beta) + \phi_1)}{2} = \frac{2\phi_1}{2} = \phi_1$$

This correction is thus applicable when the heating rate and cooling rate are the same.

Chapter 4

Results and Discussion

In this chapter all the results derived from the data collected during the experiments will be presented. The first section is dedicated to the comparison between MultiSTAR UFS and MultiSTAR UFH sensors, performed using different sizes of pure lead samples. The second section deals with the data obtained from the measurements done with pure aluminium on the MultiSTAR UFH sensors.

The results of each sample are shown separately, always preceded by the information on sensor and mass. For each sample, there will be three different kind of infographic:

- graphs presenting an overall view of the all the data:
  its aim is to understand the general trends of the measurements;
- graphs displaying only a selection of curves:
  the comparison between the more pertinent curves offers to opportunity to have a better quantitative understanding of the results;
- tables containing a more detailed quantitative analysis of the most consistent results:
  in addition to the absolute values of the C_p measurements, these tables contain also the relative difference between the literature values, expressed as a percentage.

To facilitate the understanding of the information, a constant notation is used.

Notation

The notation adopted is the following:

- Each sample is associated to a letter (e.g. *A*);
- heating and cooling rates are always expressed in K s^{-1}, and they are preceded by a letter indicating their nature (H for heating, C for cooling). In this way, H100 stands for the segment in which the sample is heated at 100 K s^{-1}, and, analogously, C100 stands for the segment in which the sample is cooled at 100 K s^{-1}.
- Each heating rate is expressed with one single colour, ranging from dark (slowest) to light (fastest).
- The type of line expresses the nature of the curve:
    - Raw data are represented by a dotted line;
    - Symmetry correction data are represented by a regular line;
    - Slow correction data are represented by a dashed/dotted line.
    - Literature values are always represented by a red line.

This page is intentionally left blank.

Sample	Metal	Mass	Sensor
I	Pb	5,17 µg	UFS 42960

As described in figure Fig. 4.1, most of the data fit the literature C_p trend, except for *row* data of the 100 K/s measurements.

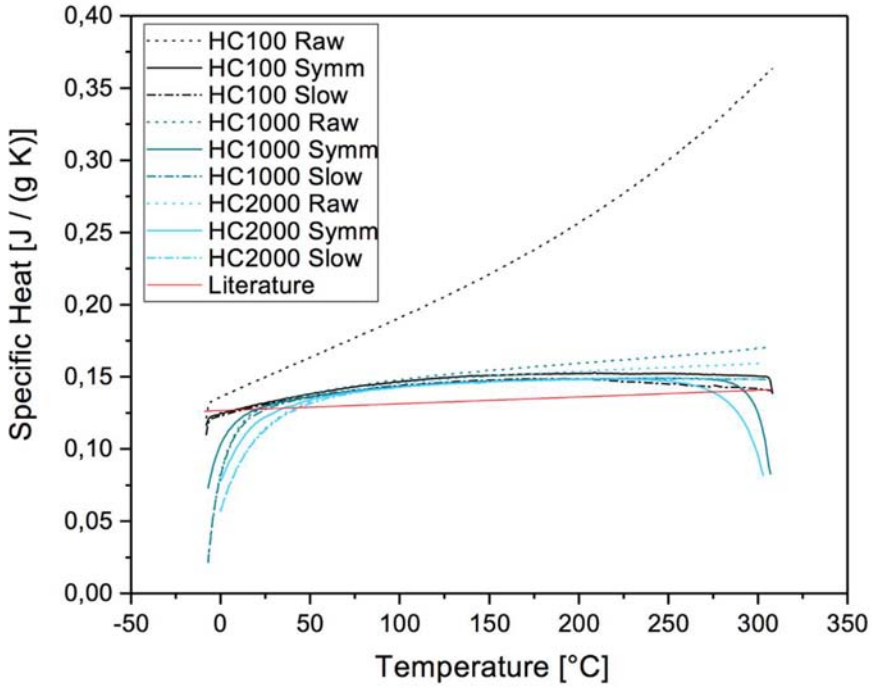

Fig. 4.1 - Sample I, all curves.

Analysing the more consistent curves, it is found the following behaviour:

- The corrective methods enhance the precision compared to raw data;
- Both slow correction and symmetry correction values are similar, with a trend of improvement when increasing the heating rate.

Sample	Metal	Mass	Sensor
I	Pb	5,17 µg	UFS 42960

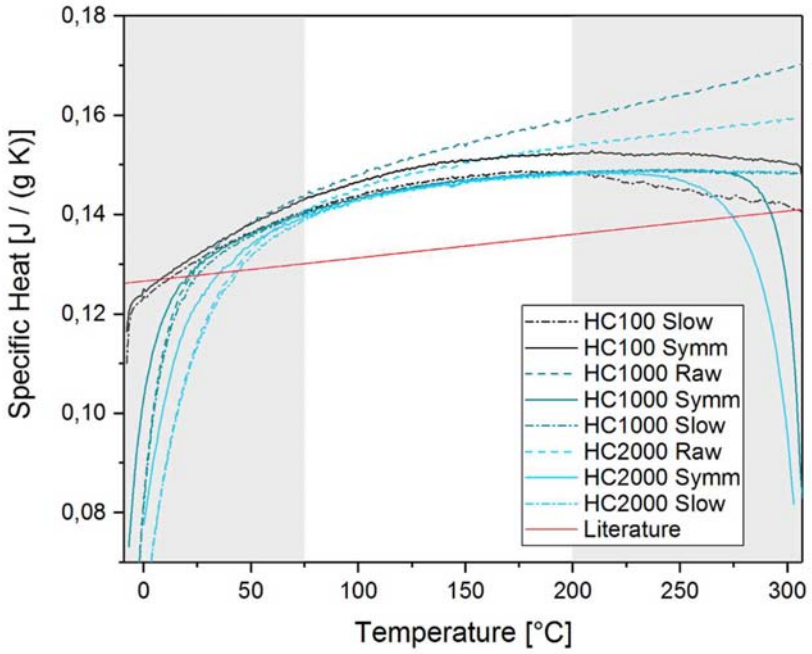

Fig. 4.2 - Sample I, selection of curves.

Tab. 4.1 - Sample I, quantitative analysis of the selected curves.

	Curve		$\Delta_{literature}$	linear
---	HC100	Symm	+12,17 %	No
---	HC100	Slow	+9,92 %	No
---	HC1000	Raw	+14,56 %	Yes
---	HC1000	Symm	+9,44%	Yes
---	HC1000	Slow	+9,46%	Yes
---	HC2000	Raw	+11,74%	Yes
---	HC2000	Symm	+9,09%	Yes
---	HC2000	Slow	+9,19%	Yes

H=Heating, C=Cooling; Range 75 / 200 °C

Sample	Metal	Mass	Sensor
L	Pb	2,117 µg	UFS 42965

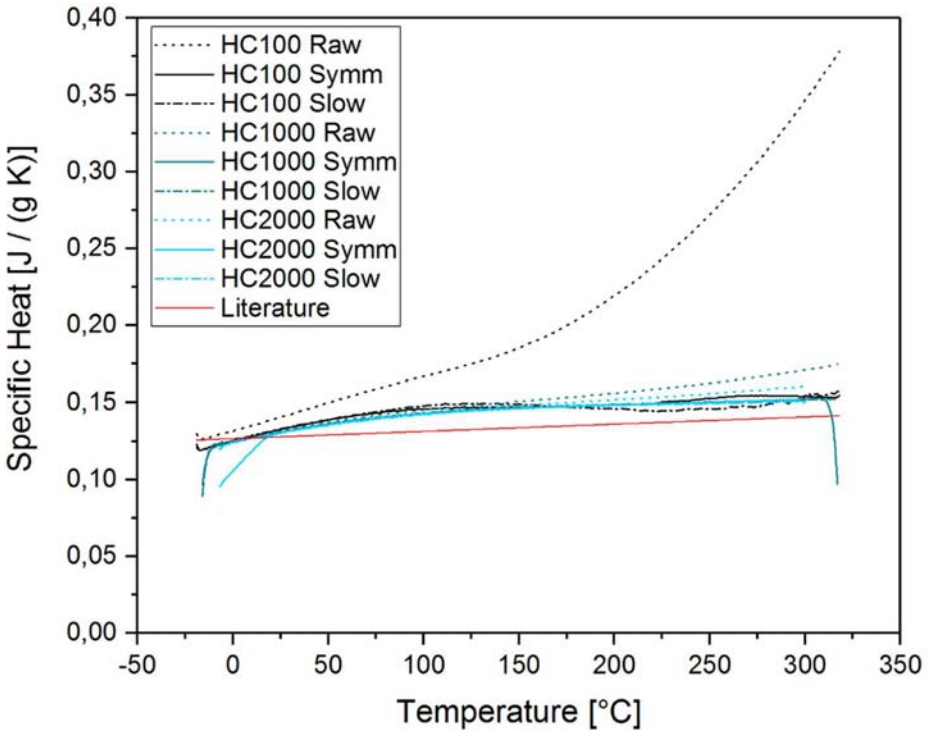

Fig. 4.3 - Sample L, all curves.

Even if sample L has halved mass compared to the previous sample, I, the results are similar. Row data deviate more from literature values, especially at high temperatures. The corrective methods are 1,5 – 2% more accurate than the raw data, but their slope better represent the specific hit, and it is kept until the end of the measurement.

The best results are obtained at 2000 K/s, with a deviation from the literature values nearby 9%.

Sample	Metal	Mass	Sensor
L	Pb	2,117 µg	UFS 42965

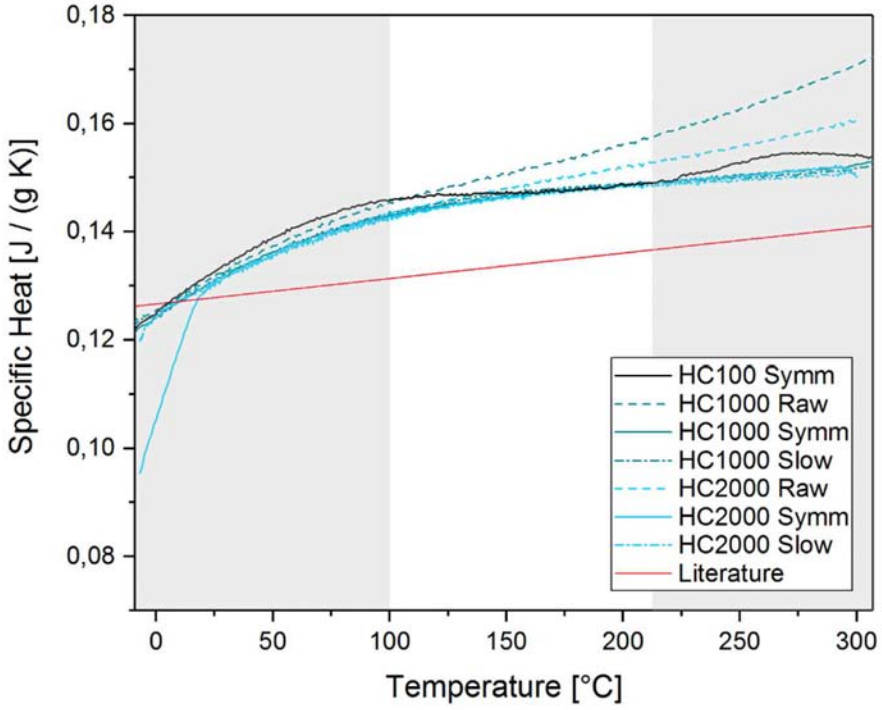

Fig. 4.4 - Sample L, selection of curves.

Tab. 4.2 - Sample L, quantitative analysis of the selected curves.

	Curve		$\Delta_{literature}$	linear
---	HC100	Symm	+9,93%	No
---	HC1000	Raw	+13,26%	Yes
---	HC1000	Symm	+9,37%	Yes
---	HC1000	Slow	+9,63%	Yes
---	HC2000	Raw	+10,85%	Yes
---	HC2000	Symm	+9,26%	Yes
---	HC2000	Slow	+9,04%	Yes

H=Heating, C=Cooling; Range 100 / 225 °C

Sample	Metal	Mass	Sensor
H	Pb	1,234 µg	UFS 42962

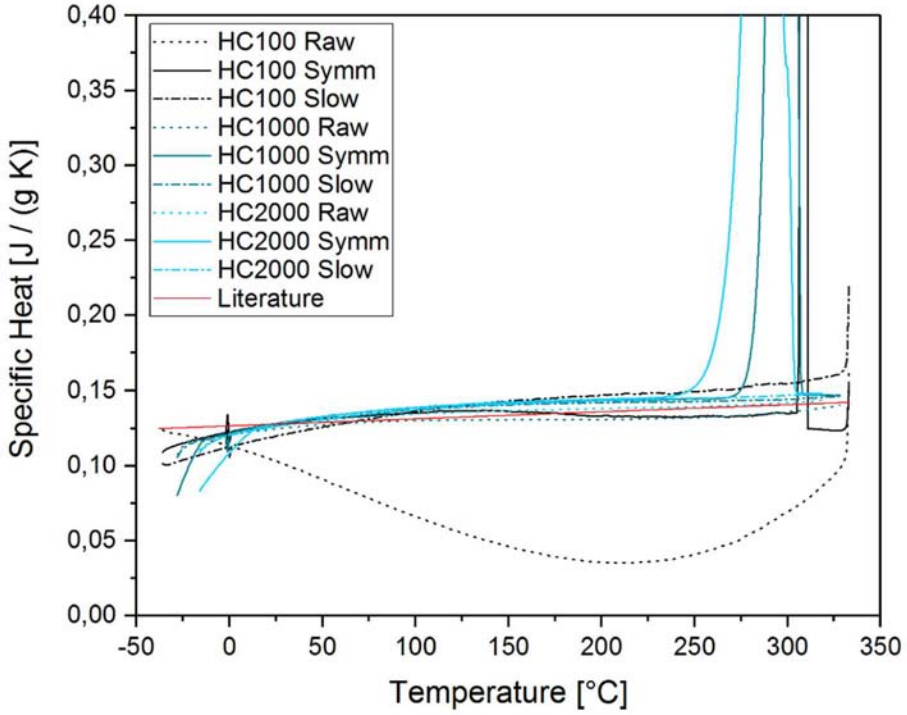

Fig. 4.5 - Sample H, all curves.

In absolute terms, the best value of specific heat for the sample H are obtained from the raw data. Nevertheless, the corrective methods increase the quality of the slope, producing specific heat curves with a slope that better resemble the literature values. Both for HC1000 and HC2000 corrective methods values the difference consist in a +5% compared to literature.

Sample	Metal	Mass	Sensor
H	Pb	1,234 µg	UFS 42962

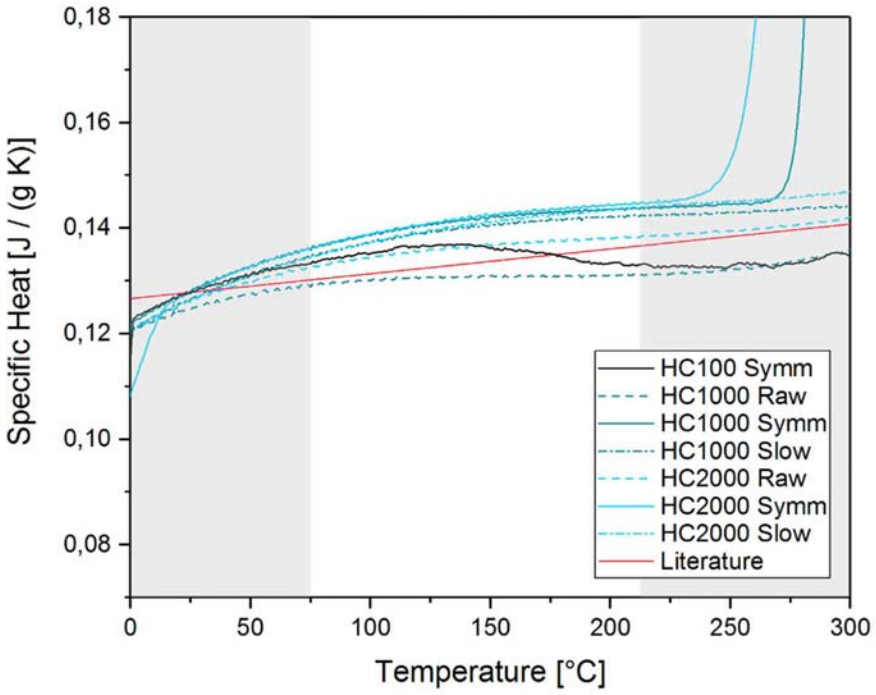

Fig. 4.6 - Sample H, selection of curves.

Tab. 4.3 - Sample H, quantitative analysis of the selected curves.

	Curve		$\Delta_{literature}$	linear
---	HC100	Symm	0,99%	No
---	HC1000	Raw	-2,28%	Yes
---	HC1000	Symm	+5,75%	Yes
---	HC1000	Slow	+4,66%	Yes
---	HC2000	Raw	+2,04%	Yes
---	HC2000	Symm	+6,08%	Yes
---	HC2000	Slow	+5,15%	Yes

H=Heating, C=Cooling; Range 75 / 225 °C

Sample	Metal	Mass	Sensor
E	Pb	0,225 µg	UFS 42965

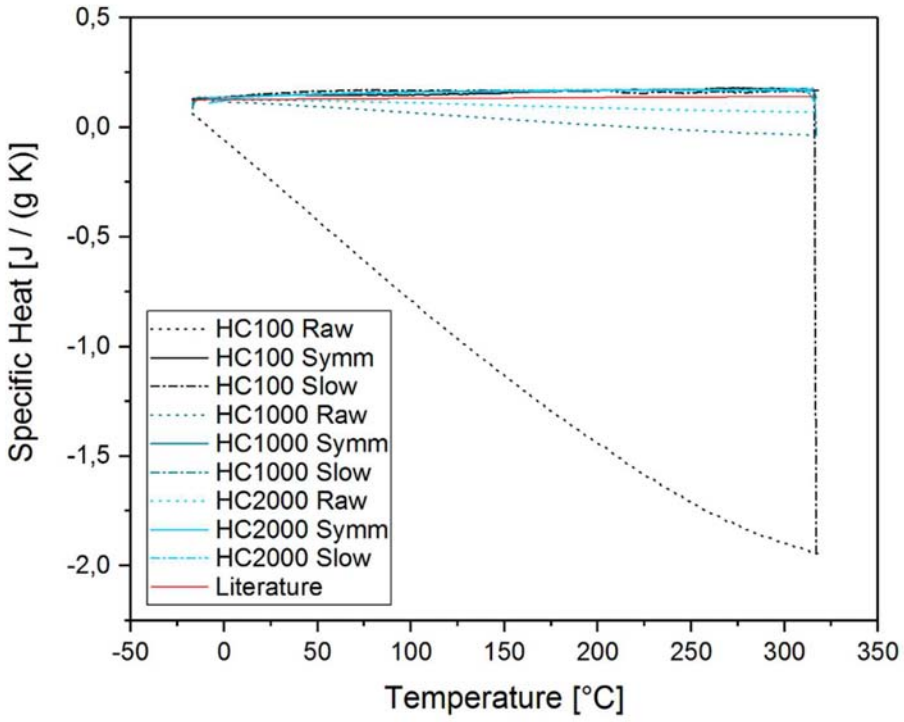

Fig. 4.7 - Sample E, all curves.

Sample E has a mass of 0,225, making the sensor work to its lower end of its sensibility.

Raw data perform poorly compared to the corrective methods, and at the same time both slow correction and symmetry correction deviate from literature values of about 23%. This result is markedly not in line with the previous ones. The slope well represents the literature values, suggesting that mass determination could play an important role.

Sample	Metal	Mass	Sensor
E	Pb	0,225 µg	UFS 42965

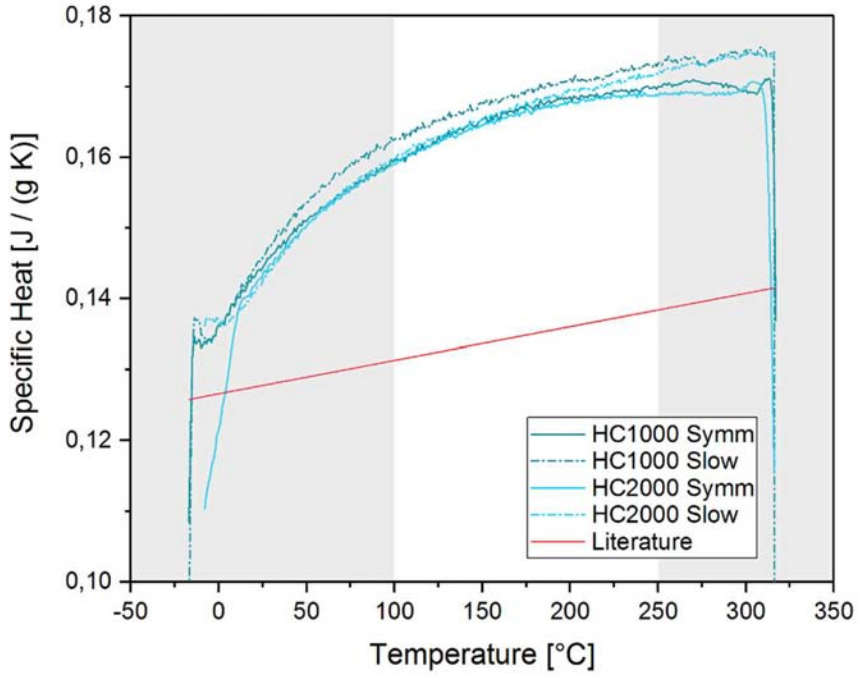

Fig. 4.8 - Sample E, selection of curves.

Tab. 4.4 - Sample E, quantitative analysis of the selected curves.

Curve			$\Delta_{literature}$	linear
---	HC1000	Symm	+23,18%	Yes
---	HC1000	Slow	+25,10%	Yes
---	HC2000	Symm	+22,79%	Yes
---	HC2000	Slow	+23,75%	Yes

H=Heating, C=Cooling; Range 100 / 250 °C

Sample	Metal	Mass	Sensor
C	Pb	0,004 µg	UFS 42965

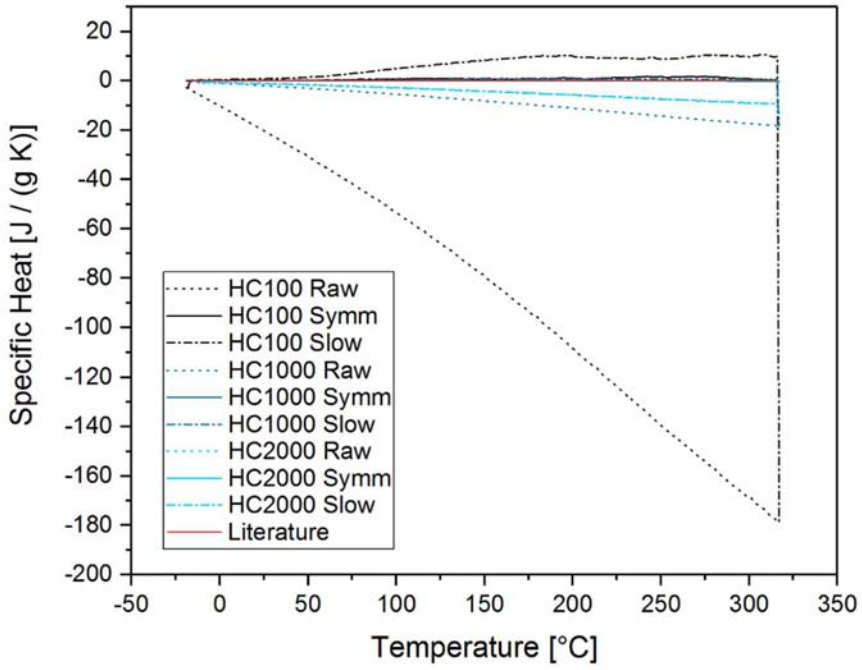

Fig. 4.9 - Sample C, all curves.

Sample C wants to take to the extreme the capabilities of the sensor: its weigh its is of only 4 ng. The melting peak is clearly recognizable (Fig. 4.10), and the temperature of melting measured is 3°C lower that the literature (-1%). While it is possible to have a good evaluation of the temperature of melting, the same cannot be said about the specific heat.

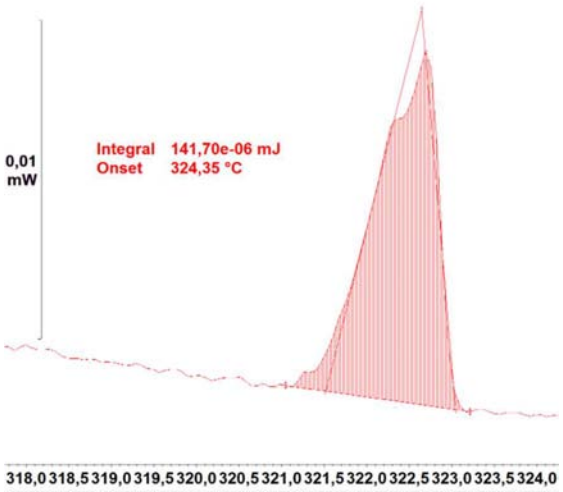

Fig. 4.10 - Sample C, melting peak.

Sample	Metal	Mass	Sensor
C	Pb	0,004 µg	UFS 42965

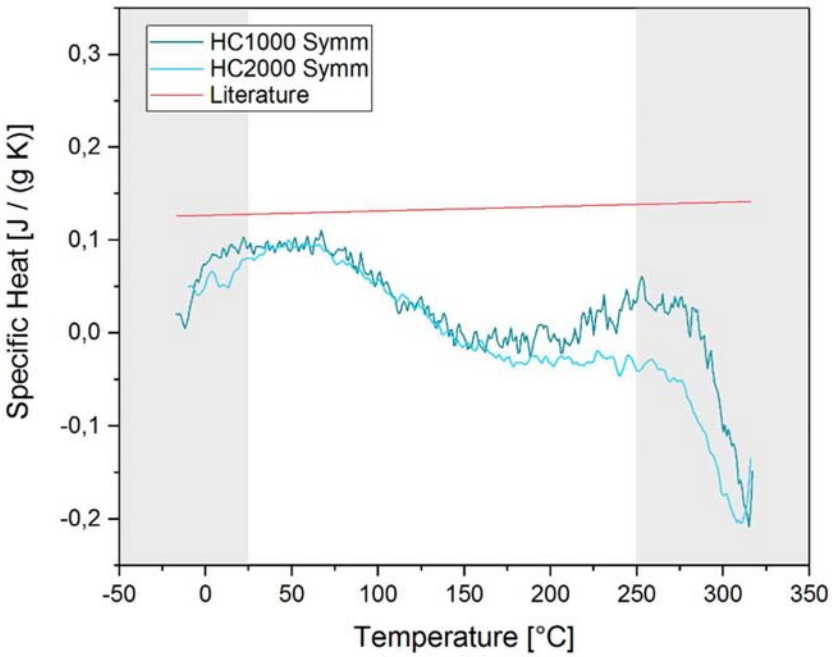

Fig. 4.11 - Sample C, selection of curves.

The best curves, derived from the symmetry correction, poorly resemble the literature values and, most of all, they do not have the characteristic slope of Lead. Their lack of linearity together with relative values of -72% and -84% make the measurement of such a small sample unsuccessful, in terms of specific heat.

Tab. 4.5 - Sample C, quantitative analysis of the selected curves.

	Curve		$\Delta_{literature}$	linear
---	HC1000	Symm	-72,72%	No
---	HC2000	Symm	-84,00%	No

H=Heating, C=Cooling; Range 25 / 250 °C

Sample	Metal	Mass	Sensor
N	Pb	0,066 µg	UFH 47912

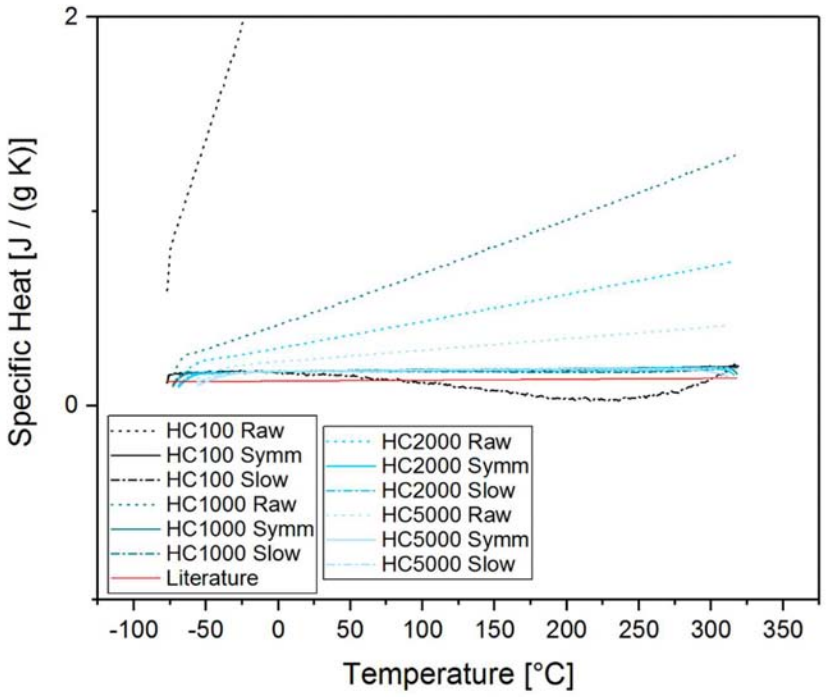

Fig. 4.12 - Sample N, all curves.

Sample N is the first Pb sample analysed on the MultiSTAR UFH 1 sensor.

Corrective methods improve the quality of the results at any speed. In Fig. 4.12 it is possible to observe how the increase of the heating rate enhance the quality of the raw data, by reducing the influence of P_{loss} as explained in paragraph 3.2.3.

Slow correction data are less linear than the symmetry corrected data, because of a lack of linearity of the slow curve which affects the results.

Symmetry correction data are linear, and slope is in line with the literature. Unfortunately, none of these curves get closer than +40% compared to literature values.

Sample	Metal	Mass	Sensor
N	Pb	0,066 µg	UFH 47912

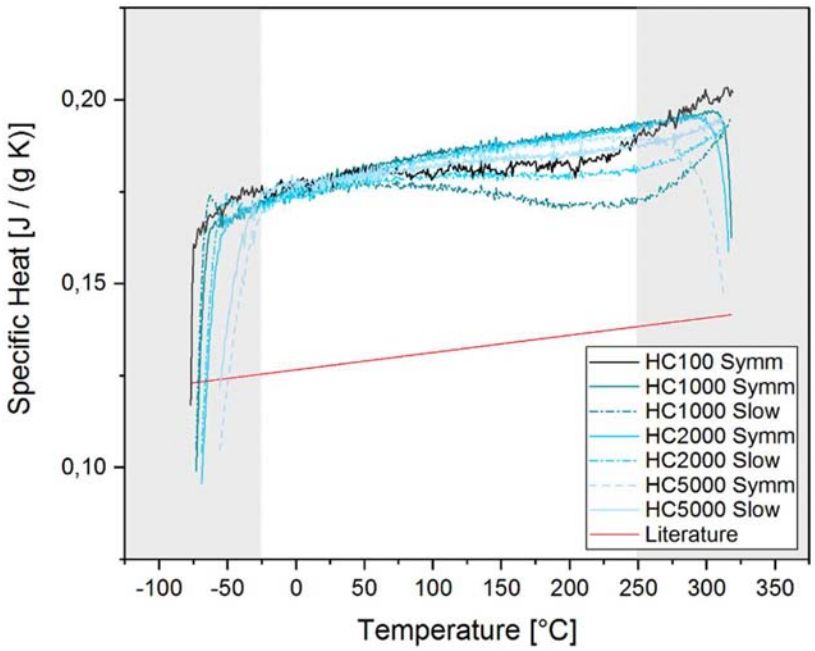

Fig. 4.13 - Sample N, selection of curves.

Tab. 4.6 – Sample N, quantitative analysis of the selected curves.

Curve			$\Delta_{literature}$	linear
---	HC100	Symm	+37,20%	No
---	HC1000	Symm	+40,21%	Yes
---	HC1000	Slow	+32,30%	No
---	HC2000	Symm	+39,50%	Yes
---	HC2000	Slow	+35,08%	Yes
---	HC5000	Symm	+39,05%	Yes
---	HC5000	Slow	+37,98%	Yes

H=Heating, C=Cooling; Range -25 / 250 °C

Sample	Metal	Mass	Sensor
P	Pb	0,043 µg	UFH 47918

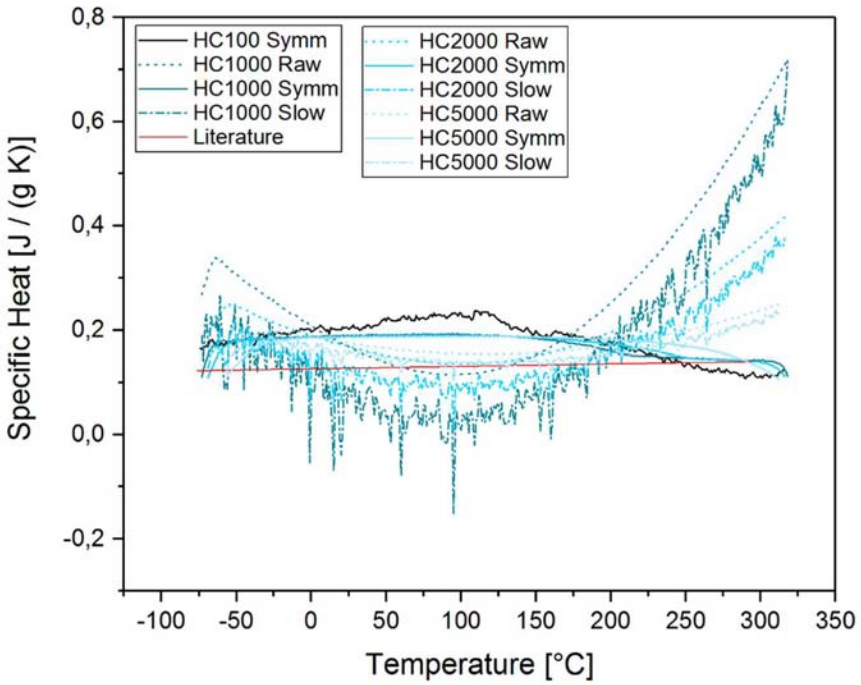

As regards sample P, both row data and slow correction data do not have a linear behaviour. Analogously to sample N, all the symmetry correction data are about +40 % compared to the literature.

The only exception is represented by the slow correction curve obtained at HC5000 K/s, but its nature is poorly linear, and thus less reliable.

Sample	Metal	Mass	Sensor
P	Pb	0,043 µg	UFH 47912

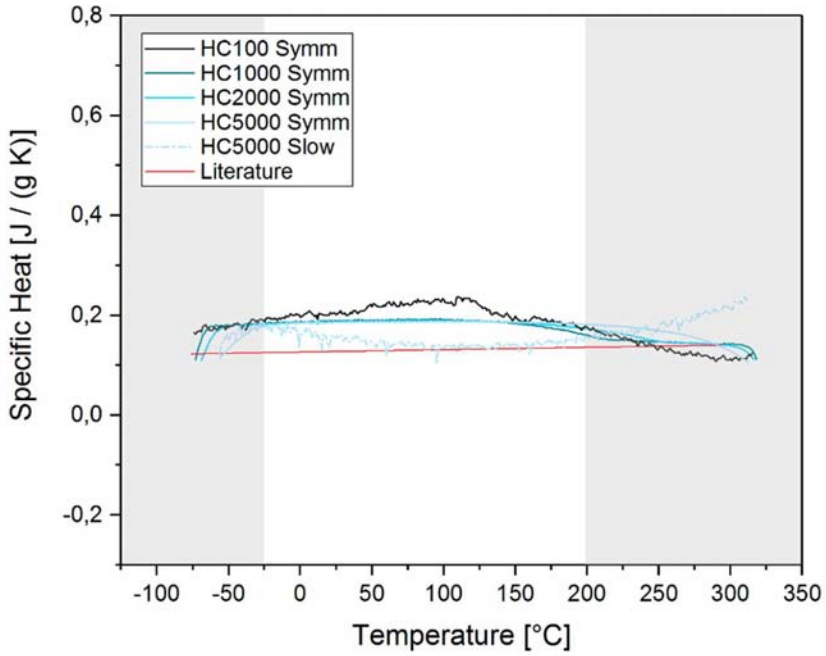

Fig. 4.14 - Sample P, selection of curves.

Tab. 4.7 - Sample P, quantitative analysis of the selected curves.

Curve			$\Delta_{literature}$	linear
---	HC100	Symm	+58,21%	No
---	HC1000	Symm	+41,97%	Yes
---	HC2000	Symm	+42,14%	Yes
---	HC5000	Symm	+42,24%	Yes
---	HC5000	Slow	+12,97%	No

H=Heating, C=Cooling; Range -25 / 200 °C

Sample	Metal	Mass	Sensor
S	Pb	2,009 µg	UFH 47911

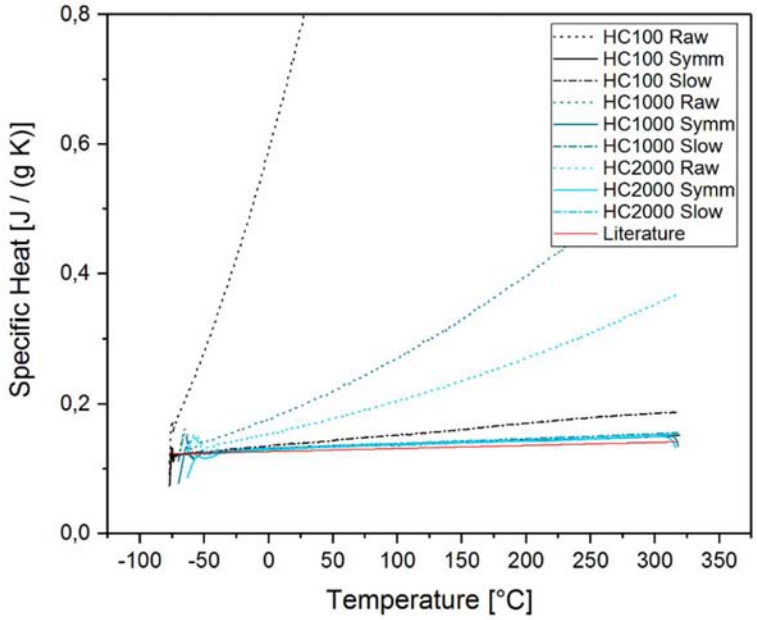

Fig. 4.15 - Sample S, all curves.

Sample S has a weight (2,009 µg) almost identical to sample L (2,117 µg), the sample measured on a MultiSTAR UFS 1 sensor.

Row data strongly deviate from literature values, but the results of the two corrective methods well resemble literature values. Symmetry correction methods performs slightly better than slow correction methods (+4,93% and +4,77% vs. +6,97% and +6,29%).

The slope is in line with literature values.

Sample	Metal	Mass	Sensor
S	Pb	2,009 µg	UFH 47911

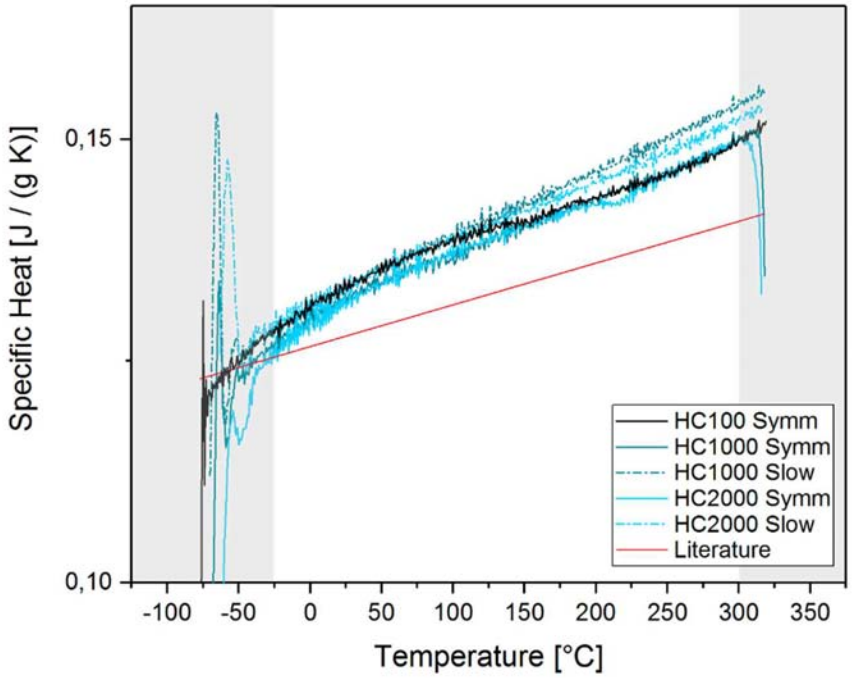

Fig. 4.16 - Sample S, selection of curves.

Tab. 4.8 - Sample S, quantitative analysis of the selected curves.

	Curve		$\Delta_{literature}$	linear
---	HC100	Symm	+5,42%	Yes
---	HC1000	Symm	+4,93%	Yes
---	HC1000	Slow	+6,97%	Yes
---	HC2000	Symm	+4,77%	Yes
---	HC2000	Slow	+6,29%	Yes

H=Heating, C=Cooling; Range -25 / 300 °C

Sample	Metal	Mass	Sensor
U	Al	0,148 µg	UFH 48431

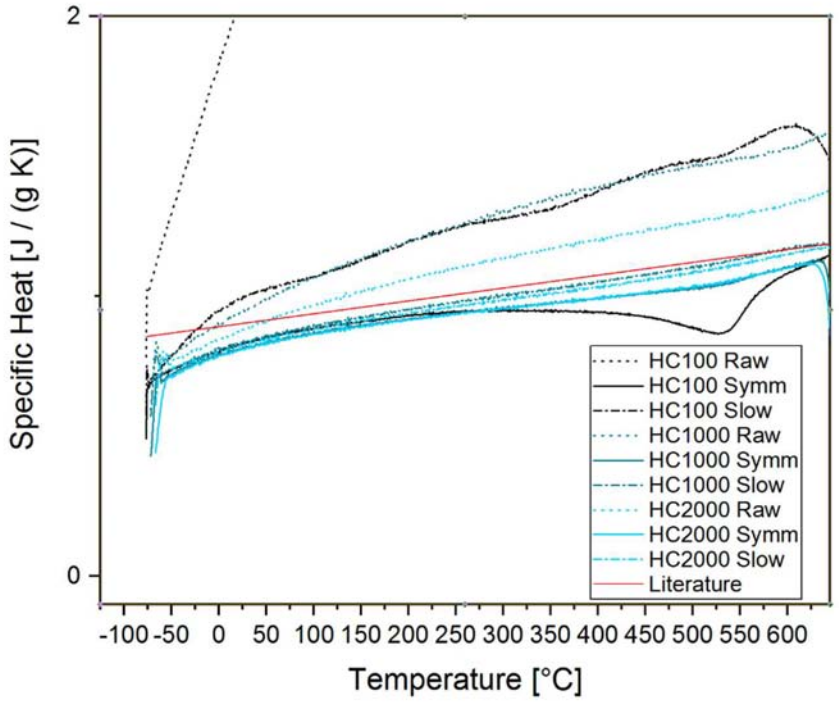

Fig. 4.17 - Sample U, all curves.

Sample U is the first Al sample analysed on a MultiSTAR UFH 1 sensor.

Raw data increase the accuracy with the increase of the heating rate, shifting from +25% for the row HC1000 to +9% for the row HC2000.

The most interesting results are obtained from the corrective methods: even though the best match with literature values is given by the slow correction method (-2,7%, -4,2%), the slope of the curves obtained with the symmetry correction method better resemble the slope of the literature values. Symmetry corrected curves differs from literature values by a -7,3%.

Sample	Metal	Mass	Sensor
U	Al	0,148 µg	UFH 48431

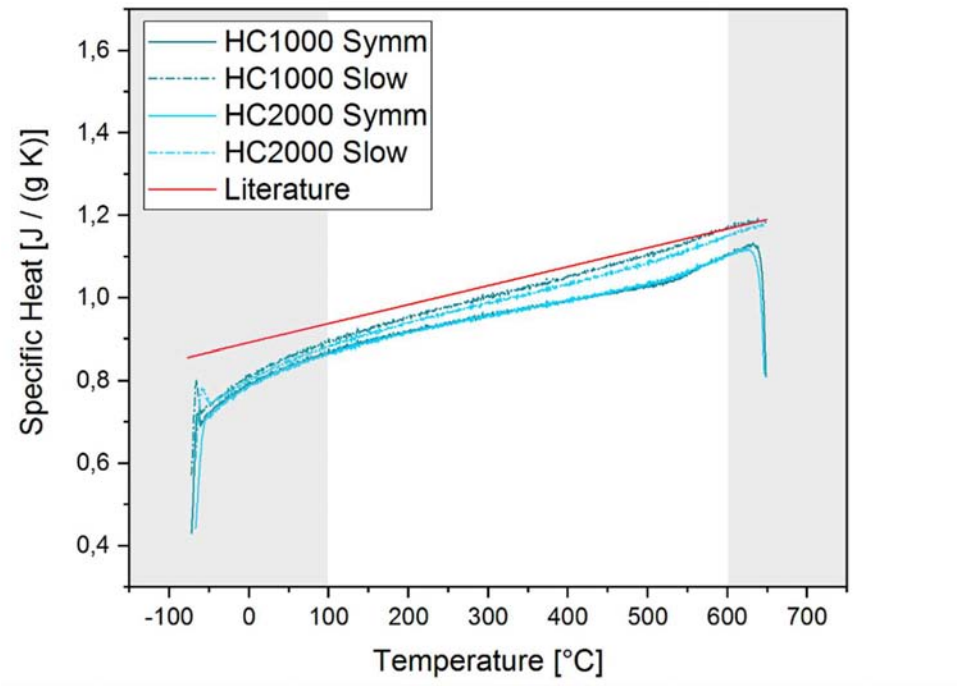

Fig. 4.18 - Sample U, selection of curves.

HC1000 Raw = +25,39%

HC2000 Raw = +9,85 %

Tab. 4.9 – Sample U, quantitative analysis of the selected curves.

Curve			$\Delta_{literature}$	linear
---	HC1000	Symm	-7,30%	Yes
---	HC1000	Slow	-2,70%	Yes
---	HC2000	Symm	-7,35%	Yes
---	HC2000	Slow	-4,20%	Yes

H=Heating, C=Cooling; Range 100 / 600 °C

Sample	Metal	Mass	Sensor
Y	Al	0,294 µg	UFH 48435

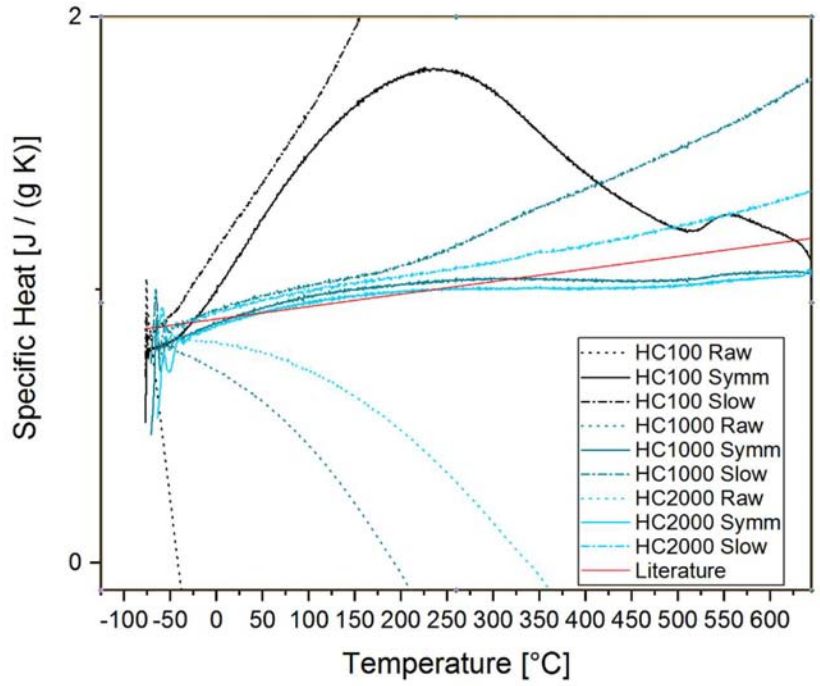

Fig. 4.19 - Sample Y, all curves.

Sample Y's mass is twice the mass of sample U. The data originated from these measurements shows no consistency, most of all because a lack of linearity compared to the other experiments.

Sample	Metal	Mass	Sensor
Y	Al	0,294 µg	UFH 48435

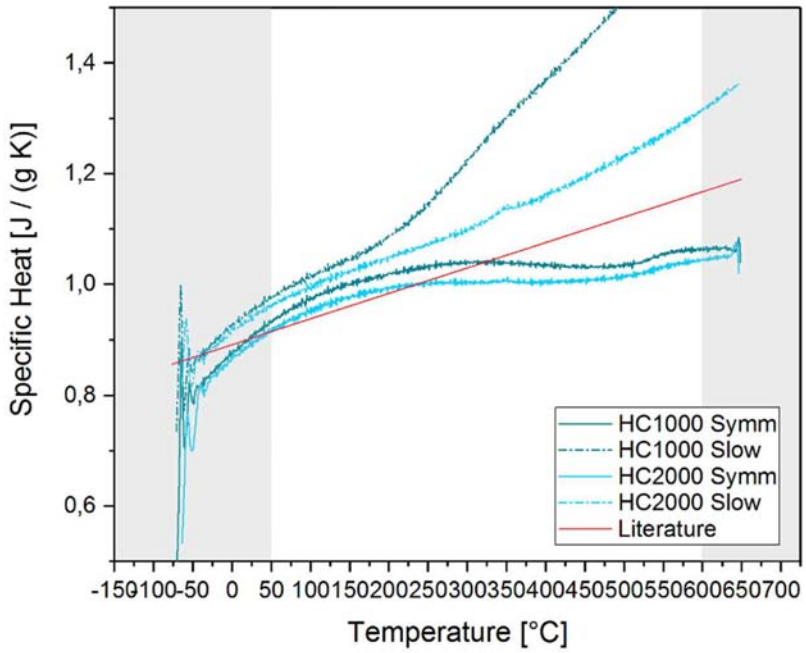

Fig. 4.20 – Sample Y, selection of curves.

Tab. 4.10 – Sample Y, quantitative analysis of the selected curves.

	Curve		$\Delta_{literature}$	linear
---	HC1000	Symm	+-1,37	No
---	HC1000	Slow	+21,96	No
---	HC2000	Symm	-3,89%	Yes
---	HC2000	Slow	+7,90%	No

H=Heating, C=Cooling; Range 50 / 600 °C

Sample	Metal	Mass	Sensor
Z	Al	0,490 µg	UFH 47904

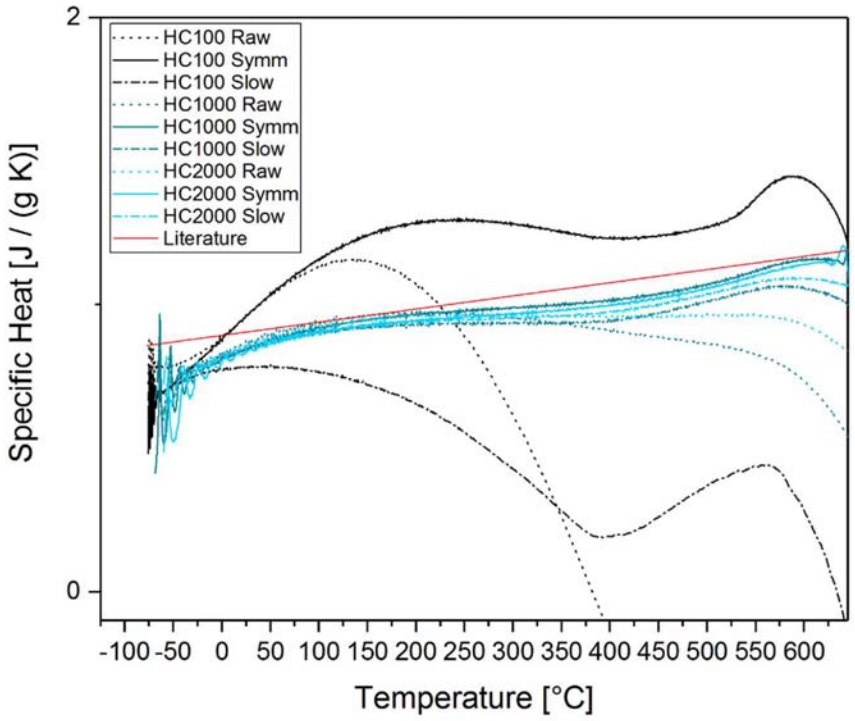

Fig. 4.21 – Sample Z, all curves.

Sampe Z is placed on a MultiSTAR UFH 1 sensor with a carbon coating deposed on its surface. Aim of this coating is to lubricate the surface, reducing tensions and allowing a possible detachment of the sample after the measurement.
Even though the results of the symmetry correction method are between -3,5% and -5,2%, the quality of the slope is inferior to the one of the curves obtained with sample U.

Sample	Metal	Mass	Sensor
Z	Al	0,490 µg	UFH 47904

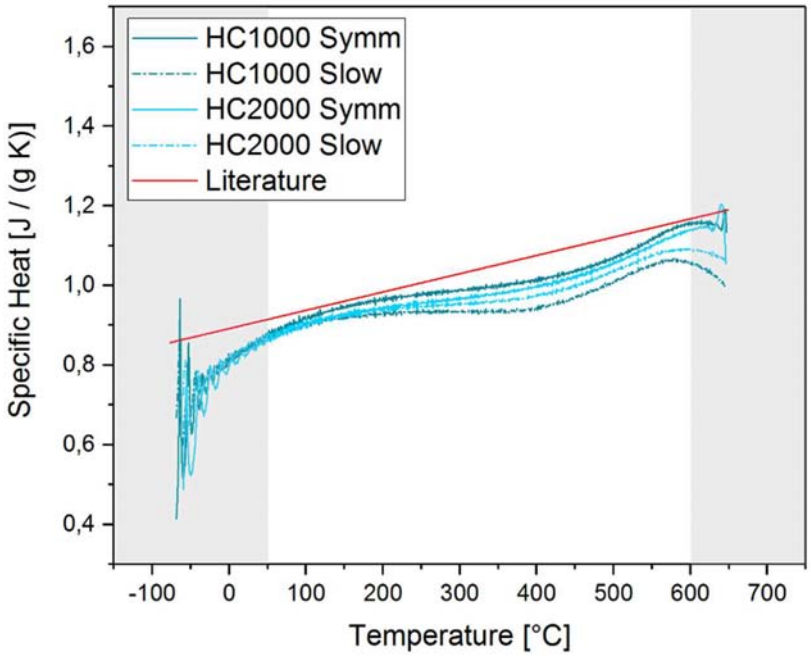

Fig. 4.22 - Sample Z, selection of curves.

Tab. 4.11 - Sample Y, quantitative analysis of the selected curves.

	Curve		$\Delta_{literature}$	linear
---	HC1000	Symm	-3,51%	Yes
---	HC1000	Slow	-8,20%	No
---	HC2000	Symm	-5,22%	Yes
---	HC2000	Slow	-6,46%	No

H=Heating, C=Cooling; Range 50 / 600 °C

Conclusion

Raw data, particularly at high rates, can sometimes offer a good approximation of the specific heat. The corrective methods proved to always offer an enhancement of the quality of the specific heat measurements.

Generally, slow correction and symmetry correction give both better results, compared to the raw data. But among the two, symmetry correction has shown to provide the best results in terms of slope, and it is also the more constant method: the effectiveness of the obtained results has been always maintained in all the experiments.

Slow correction, although many times match the symmetry correction, is affected by the quality of the slow measurement. In case of a low-quality measurement, the results are affected consequently.

The slope of the measured curves well fits the slope of the literature in most cases: the mass determination could play a role in the precision of results. If the mass could be measured more precisely, it could be that the gap among measured and literature values could reduce.

In addition to its relative contribute, the entity of the mass plays a role into the specific heat evaluation. Experiments performed on the MultiSTAR UFS 1 sensor show a trend of improvement when the mass goes toward 1 µg. Further experiments with masses slightly lower than 1 µg should be performed, in order to find the optimum value of mass.

As regards MultiSTAR UFH 1, it has shown that its optimum mass is around the micrograms too, even though its active area is 25 times smaller than MultiSTAR UFS 1 sensor.

Among same mass (2 µg) samples measured on MultiSTAR UFS 1 and MultiSTAR UFH 1, the latter showed similar results (+4,8% for the HC2000 symmetry corrected), compared to MultiSTAR UFS 1 (+6,1% for the HC2000 symmetry corrected).

All the things that have been said for the lead remain valid also for aluminium. Further studies should be performed on the use of carbon sputtered film as a lubricant medium, since the results obtained with sample Z don’t differ significantly from the carbon film-free measurements.

Acknowledgements

I would like to express my thanks to Prof. Stefan Pogatscher, both for giving me the opportunity of working on such an advanced instrument like it is the Flash DSC 2+, but most of all for having transmitted to me the fresh enthusiasm that only the passion for research can give.

I'm deeply indebted to Cameron Quick, who trained me and supported me throughout the duration of the exchange.

Thanks also to Dr. Florian Spieckermann, from the Eric Schmid Institute, for the valuable advice.

Sincere thanks also to Prof. Helmut Antrekowitsch, and to all the staff of the Lehrsthul für Nichteisenmetallurgie: I am grateful for your warm welcome, and your availability helped me and meant a lot for me.

I'm also grateful to Prof. Irene Calliari, whose Erasmus Exchange allowed me to work on my thesis and live for 5 wonderful months in Austria.

A heartfelt thanks to my family, I cannot imagine who would I be without you.

Last but not least, I would like to thank all the friends from the student residence who made me feel like home, and to all the people back home who have always been unconditionally by my side in recent years.

References

[1] R. C. Mackenzie, “Origin of Thermal Analysis,” *Isr. J. Chem.*, vol. 22, no. 3, pp. 203–205, 1982, doi: 10.1002/ijch.198200040.

[2] A. Fortunato, *DSC: History, instruments and devices*. Woodhead Publishing Limited, 2013.

[3] H. Le Chatelier, “De l ’action de la chaleur sur les argiles,” vol. 10, pp. 204–211, 1887.

[4] W. C. Roberts-Austen, “Fifth Report to the Alloys Research Committee: Steel,” 1899.

[5] E. S. Watson, M. J. O’Neill, J. Justin, and N. Brenner, “A Differential Scanning Calorimeter for Quantitative Differential Thermal Analysis,” *Anal. Chem.*, vol. 36, no. 7, pp. 1233–1238, 1964, doi: 10.1021/ac60213a019.

[6] C. Schick and V. Mathot, Eds., *Fast Scanning Calorimetry*. Cham: Springer International Publishing, 2016.

[7] E. Zhuravlev and C. Schick, “Fast scanning power compensated differential scanning nano-calorimeter: 1. The device,” *Thermochim. Acta*, vol. 505, no. 1–2, pp. 1–13, 2010, doi: 10.1016/j.tca.2010.03.019.

[8] Mettler Toledo, “Flash DSC 2+: User Manual.” p. 103, 2018.

[9] E. Iervolino *et al.*, “Temperature calibration and electrical characterization of the differential scanning calorimeter chip UFS1 for the Mettler-Toledo Flash DSC 1,” *Thermochim. Acta*, vol. 522, no. 1–2, pp. 53–59, 2011, doi: 10.1016/j.tca.2011.01.023.

[10] DIN SPEC 91127:2011-06, “Recommendation for Temperature Calibration of Fast Scanning Calorimeters (FSCs) for Sample Mass and Scan Rate.” 2011.

[11] W. F. Gale and T. C. Totemeier, *Smithells Metals Reference Book*, 8th ed. Elsevier Butterworth-Heinemann, 2004.

[12] С. Ю. Марцевич and В. И. Метелица, “Изосорбида динитрат: зависимость антиангинального эффекта от лекарственной формы и дозы препарата No Title,” *Тер.*

Apx., vol. 60, no. 8, pp. 27–30, 1988.

[13] E. Zhuravlev and C. Schick, “Fast scanning power compensated differential scanning nano-calorimeter: 2. Heat capacity analysis,” *Thermochim. Acta*, vol. 505, no. 1–2, pp. 14–21, 2010, doi: 10.1016/j.tca.2010.03.020.

List of Tables

List of Figures